RSC Advances

PAPER

View Article Online
View Journal | View Issue

Cite this: *RSC Adv.*, 2024, **14**, 18838

Design, synthesis, and anticancer evaluation of novel coumarin/thiazole congeners as potential CDK2 inhibitors with molecular dynamics†

Samir Bondock, *[a] Nada Alabbad,[a] Aisha Hossan,[a] Moaz M. Abdou,[b] Ali A. Shati,[c] Mohammad Y. Alfaifi,[c] Serag E. I. Elbehairi[c] and Nada M. Mohamed[d]

A series of novel coumarin–thiazoles was designed and synthesized as a possible CDK2 inhibitor with anticancer activity with low toxicity. The design relied on having hydrazine thiazole or its open-form thioamide to form H-bonds with the ATP binding site while coumarin maintained the crucial hydrophobic interactions for proper fitting. The biological evaluation revealed that the hydroxycoumarin-thiazole derivative **6c** demonstrated the best inhibition with HepG2 and HCT116 IC_{50} 2.6 and 3.5 μM, respectively. Similarly, its open thioamide chain congener **5c** exhibited potent inhibition on MCF-7 and HepG2 with IC_{50} of 4.5 and 5.4 μM, respectively. Molecular docking simulations supported the assumption of inhibiting CDK2 by preserving the crucial interaction pattern with the hinge ATP site and the surrounding hydrophobic (HPO) side chains. Furthermore, molecular dynamics simulations of **5c** and **6c** established satisfactory stability and affinity within the CDK2 active site.

Received 1st April 2024
Accepted 28th May 2024

DOI: 10.1039/d4ra02456g

rsc.li/rsc-advances

1. Introduction

Cancer is a multi-process disease of variable etiology that results in rapid and uncontrolled cell division with the over-expression of its relevant machinery enzymes. One of those important enzymes is the cyclin-dependent kinase family members that control the cell cycle. Cyclin-CDK2 is a member of the serine/threonine kinase family that regulates the G1/S phase of the cell cycle upon binding with the cyclin family, initiates DNA synthesis, and regulates the exit from S-phase.[1–3] Nonetheless, its overexpression was monitored in several malignancies.[4–6] Classically, the ATP binding site of CDK2 is located at the hinge region between the β-sheets N-terminal lobe and the α-helices C-terminal lobe.[7,8] Moreover, CDK2 is activated through dimerization by binding to cyclin E/A or phosphorylating its catalytic segment.[9] Binding to cyclin A facilitates the S-phase progression[10] while binding to cyclin E promotes the retinoblastoma protein phosphorylation to access the G1/S-phase (Fig. 1).[11] Structurally, there are four possible binding sites of CDK2 where only one emerges upon activation due to the consequent conformational changes.[12]

Thiazole and coumarin scaffolds have proved anticancer activity alone or hybridized in one structure, especially with the presence of hydrazine or hydrazone linkage.[13–15] Hydrazine and hydrazone moiety were reported to anticipate the overall structure of anticancer activity through the ability of their –NH to form hydrogen bonds with the targeted enzymes which enhanced the binding.[16,17]

One of the proposed mechanisms for thiazole and coumarin antiproliferative activity is through inhibition of CDK2 (Fig. 2). Compound **I** demonstrated CDK2 IC_{50} 0.93 μM through binding to the ATP-binding site by its thiazole moiety in addition to forming hydrogen bonds with the crucial Glu81 and Leu83 (PDB ID: 3QTR).[18] Moreover, compound **II** could downregulate CDK2 leading to promising anticancer effects.[13] In the same context, hybridizing coumarin and thiazole with hydrazone linkage in **IIIa–c** resulted in CDK2 IC_{50} 0.022–1.629 nM with anti-proliferative activity IC_{50} 0.0596–0.0091 μM against human cervical carcinoma HeLa cell line. The proposed binding pattern of **IIIa–c** to CDK2 through the interactions of the 2-aminothiazole moiety with the crucial leu83 backbone.[19] Furthermore, the thiazole hydrazone derivative **IV** showed CDK2 IC_{50} 0.39 μM.[20]

By investigating the binding conformation of the previously reported **III**, its thiazole and hydrazine linker showed the essential binding to ATP-binding sites Asp145 and Leu83, respectively. In contrast, its coumarin moiety demonstrated the crucial hydrophobic interactions for proper fitting to CDK2 hydrophobic side chains.[19] In this study, the effect of adding

[a]*Chemistry Department, Faculty of Science, King Khalid University, 9004 Abha, Saudi Arabia. E-mail: bondock@kku.edu.sa; bondock@mans.edu.eg*

[b]*Egyptian Petroleum Research Institute, Nasr City, 11727, Cairo, Egypt*

[c]*Biology Department, Faculty of Science, King Khalid University, 9004 Abha, Saudi Arabia*

[d]*Pharmaceutical Chemistry Department, Faculty of Pharmacy, Modern University for Technology and Information, MTI, Cairo, Egypt*

† Electronic supplementary information (ESI) available. See DOI: https://doi.org/10.1039/d4ra02456g

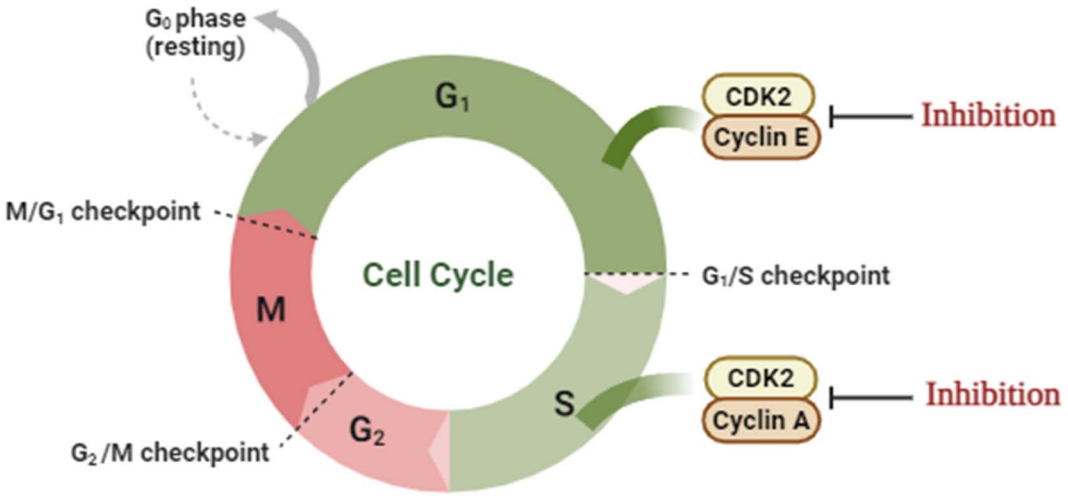

Fig. 1 An illustrative presentation of CDK2's role in the cell cycle.

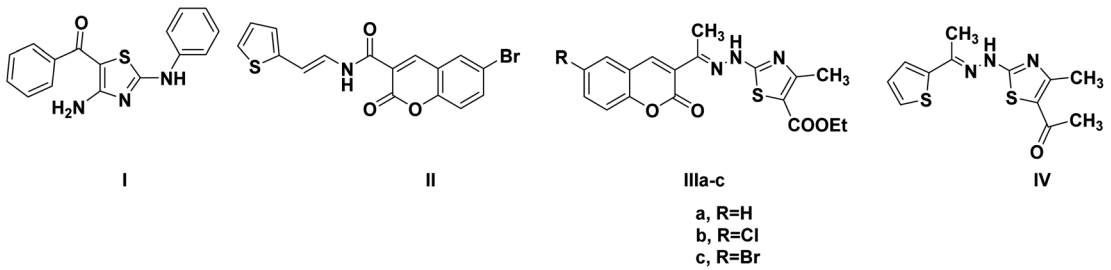

Fig. 2 Reported thiazole and coumarin-containing derivatives with CDK2 inhibitory activity.

a carbonyl group to the hydrazine linker on forming extra H-bonding with the hinge ATP region was inspected. Additionally, the impact of changing the thiazole ring into its parent open thioamide on their ability to consolidate the hinge H-bonding pattern was investigated as well in strategy A (Fig. 3). Moreover, the thiazole ring was substituted with extra phenyl moiety at C4 to achieve more hydrophobic interactions with the hinge surrounding hydrophobic regions for better fitting. On the other hand, the necessity of having a coumarin ring was evaluated by its substitution with a smaller cyano group while preserving the phenyl thiazole-carbohydrazide moiety for H-bonding and the phenyl group for the hydrophobic fitting in strategy B (Fig. 3).

2. Results and discussion

2.1. Chemistry

2.1.1. Synthesis of 1-cyanoacetylthiosemicarbazide. The commencing material, 1-cyanoacetylthiosemicarbazide **3**, was conveniently prepared by a modified method reported earlier by Balicki and Nantka-Namirski[21] *via* warming thiosemicarbazide **1** in ethanoic acid with 1-cyanoacetyl-3,5-dimethylpyrazole **2** (ref. 22) (Scheme 1). IR, ^{1}HNMR, and ^{13}CNMR spectral data recognized the molecular structure of compound **3** (ESI, Fig. S1–S3†). The IR spectrum displayed distinct absorption bands for two NH, NH_2, CN, amidic C=O, and C=S functions at frequencies 3415, 3270, 3210, 3137, 2257, 1688, and 1294 cm^{-1}, respectively. The ^{1}HNMR spectrum of **3** displayed five singlet signals resonated at δ 3.63, 7.68, 7.99, 9.35, and 10.14 ppm due to methylene protons, NH^{a}-4, NH^{b}-4, NH-2, and NH-1 protons, respectively. The ^{13}CNMR spectrum displayed four carbon signals at δ 24.73, 116.18, 162.64, and 182.32 ppm, characteristic of CH_2, CN, C=O, and C=S, respectively.

2.1.2. Synthesis of coumarin-thiazole hybrids

2.1.2.1. Synthesis of 1-(2-oxo-2H-chromene-3-carbonyl) thiosemicarbazide derivatives ***5a–d.*** Merging two bioactive pharmacophores, coumarin, and thiazole, in a single molecule may lead to the discovery of new potent anticancer agents with low toxicity. In this regard, we studied the reactivity of **3** towards sets of 2-hydroxybenzaldehydes and phenacyl bromide in a basic medium to attain some novel coumarin–thiazole hybrids. Thus, the reaction of **3** with certain sets of substituted 2-hydroxybenzaldehydes **4a–d** in the presence of piperidine afforded the corresponding thiosemicarbazide derivatives **5a–d** (Scheme 2). The IR spectra secured the molecular structures of compounds **5a–d**, revealing the absence of stretching absorption peaks of C–H sp^3 and nitrile functions (ESI, Fig. S4, S8, S11, and S17†). The characteristic absorption peaks for NH_2, NH, lactone C=O, amidic C=O, and C=S groups were seen at ranges 3404–3253, 3282–3098, 1721–1704, 1674–1651, 1273–1205 cm^{-1}, respectively. The ^{1}HNMR spectrum of coumarin **5a**, as an example, displayed two sets of three downfield singlet

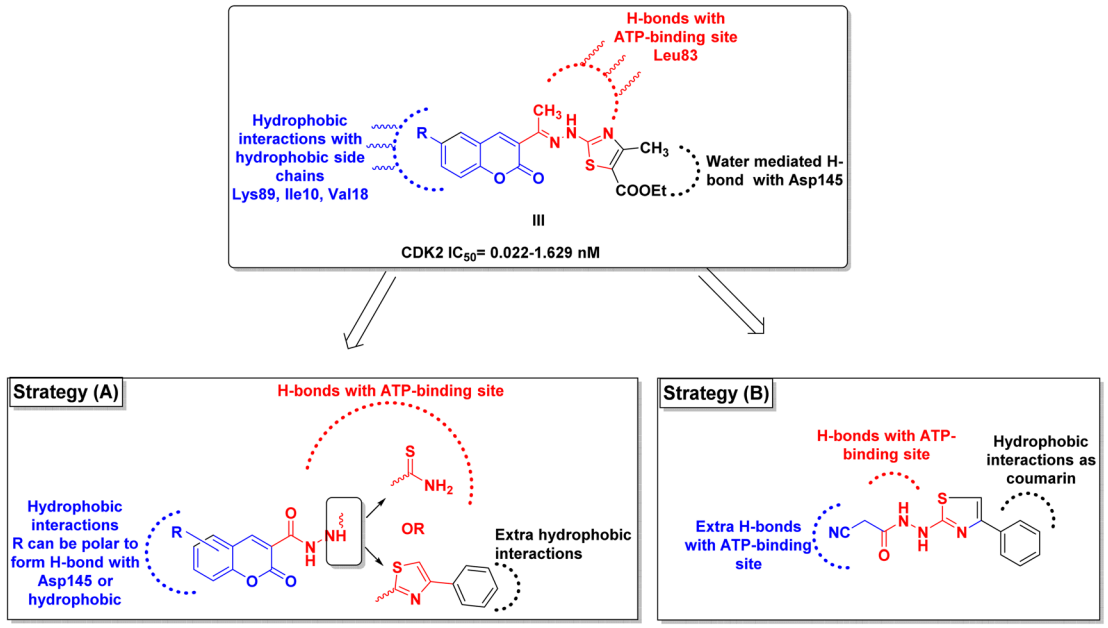

Fig. 3 Graphical presentation of the study rationale.

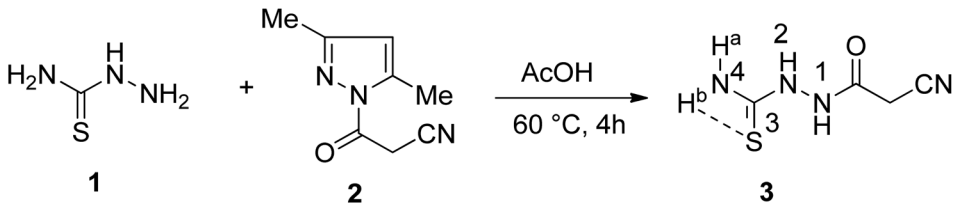

Scheme 1 Synthesis of 1-cyanoacetylthiosemicarbazide **3**.

signals at δ 9.11, 9.48 (coumarin-H4), 10.16, 10.67 (thioamide NH), and 11.52, 13.04 ppm (amidic NH), respectively. The four aromatic protons of the coumarin ring and the two magnetically nonequivalent protons of thioamide resonate at a range of δ 7.41–8.45 ppm. The appearance of doubling signals is ascribed to the existence of compound **5a** in two rotamers, *syn* and *anti*, attributed to the restricted rotation around the C–N amide bond. Based on the integration values of the more deshielded amidic proton, it is concluded that the two rotamers exist in a ratio (76 : 24). The ^{13}CNMR spectrum of **5a** revealed nine carbon peaks. The three more deshielded carbon peaks of C=S, coumarin C=O, and amidic C=O appeared at δ 182.12, 161.97, and 158.30 ppm (ESI, Fig. S9†). The mass spectra of **5a–d** revealed molecular ion peaks, which support their molecular weights in each case (ESI, Fig. S7 and S10†). Heterocyclization of thiosemicarbazides **5a–d** with 2-bromoacetophenone in the presence of triethylamine afforded coumarin–thiazole conjugates **6a–d** in good yields (70–85%) (Scheme 2).

Microanalyses and spectral data confirmed the structures of **6a–d** (ESI, Fig. S13–S27†). Their IR spectral data explored the absence of absorption bands for NH_2 and C=S functions. The characteristic absorption peaks of coumarin C=O, amidic C=O, and NH groups were seen at ranges 1715–1687, 1682–1635, and 3291–3113 cm^{-1}, respectively. For example, the ^{1}H-NMR spectrum of **6a** showed the absence of an NH_2 signal and a new singlet signal at δ 7.30 ppm due to the thiazole-H5 proton. Three peaks of the monosubstituted phenyl ring resonate at δ 7.85 (d, 2H), 7.40 (t, 2H), and 7.29 (t, 1H). Also, there are three downfield singlet signals characteristic of coumarin-H4, thiazole-NH, and amidic NH protons seen at δ 8.85, 9.92, and 10.68 ppm, respectively, besides the expected four aromatic signals of coumarin ring residue (ESI, Fig. S14†). The downfield shift signal of the amidic proton may be attributed to the formation of intramolecular hydrogen bonding with the C=O group of the coumarin ring. Its ^{13}CNMR spectrum displayed the seventeen carbon signals, which agree with its molecular structure. The most important two carbonyl carbon signals resonated at 161.98 (amidic-C=O) and 159.91 (coumarin-C=O). The thiazole carbon peaks appeared at δ 103.99, 150.94, and 171.40 ppm due to C-5, C-4, and C-2, respectively (ESI, Fig. S15†).

Conversely, the chemical structures of **6a–d** were elucidated *via* an alternative synthetic pathway. Thus, treating **3** with ω-bromoacetophenone in ethanol containing triethylamine as a base, under reflux, afforded 2-cyano-*N*′-(4-phenylthiazol-2-yl) acetohydrazide **7**. TLC checked the purity of compound **7** and its identity was confirmed by analytical and spectral data (MS, IR, ^{1}HNMR, ^{13}CNMR). The NH_2 absorption band was missed in

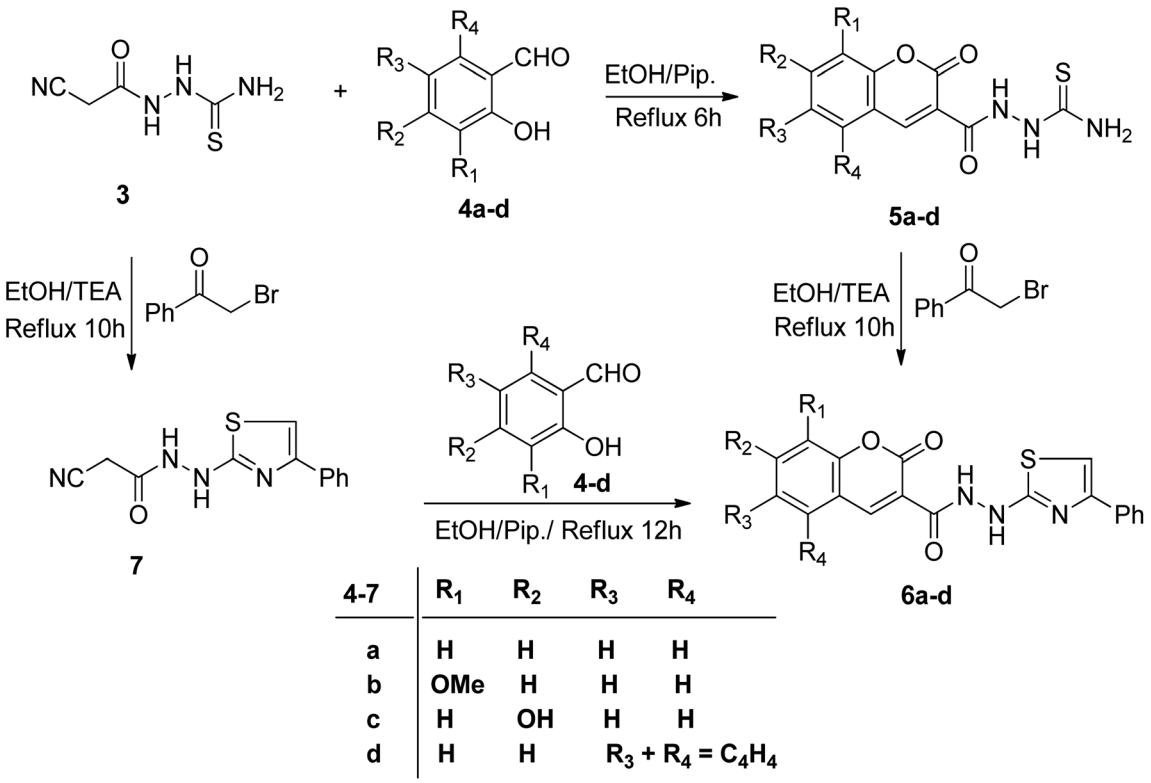

4-7	R_1	R_2	R_3	R_4
a	H	H	H	H
b	OMe	H	H	H
c	H	OH	H	H
d	H	H	$R_3 + R_4 = C_4H_4$	

Scheme 2 Synthesis of coumarin–thiazole hybrids **6a–d**.

the IR spectrum of 7 and the characteristic absorption bands were displayed at 3415, 3270, and 3195 cm^{-1} for 2nd amines and at 2257 and 1701 cm^{-1} for nitrile and amidic C=O functions, respectively (ESI, Fig. S28†). In the ^{1}HNMR spectrum of compound 7 characteristic doubling of signals for CH_2, thiazole-NH, and amidic NH is noted that corresponds to the existence of two conformers, *syn* and *anti*, a common feature of amide compounds because of restricted rotation about the C–N amide bond. Based on the integration values of methylene protons that appeared at δ 3.82, and 3.92 ppm in the ^{1}HNMR spectrum of **7**, the two isomers exist in a ratio (84 : 16) (ESI, Fig. S29†). The ^{13}CNMR spectrum of compound 7 also showed a paring of ten carbon peaks which agree with its molecular structure and support the existence of two rotamers. The more intense characteristic carbon peaks resonate at δ 24.36, 116.24, and 163.71 ppm due to the carbons of methylene, nitrile, and amidic C=O, respectively. The thiazole carbon peaks were seen at δ 103.95 (C-5), 151.42 (C-4), and 171.76 ((C-2) ppm) (ESI, Fig. S30†). Heterocyclization of the cyanoacetamide moiety of 7 with a series of 2-hydroxybenzaldehyde derivatives **4a–d** in refluxing ethanol containing one drop of piperidine as a base afforded compounds that are consistent with coumarin–thiazole conjugates **6a–d** in all aspects (MP, TLC, IR, NMR, MS). The mass fragmentation pattern of compound **6c** (ESI, Fig. S31†). As an example of the series prepared, is depicted in Scheme 3.

2.1.3. Conformation analysis of coumarin and thiazole amides. Amide compounds possess a distinct characteristic: the C–N bond exhibits a partial double bond character, impeding rotation around it. This phenomenon contrasts with typical single bonds like the C–C bond in ethane, where the rotational barrier requires about 3 kcal mol^{-1}, or the C=C bond in 2-butene, which needs about 39 kcal mol^{-1}. In comparison, the C–N bond in methyl *N*,*N*-dimethylcarbamate necessitates approximately 15 kcal mol^{-1}.[23–25] Consequently, while amide bonds don't allow for free rotation akin to single bonds, they aren't as rigid as double bonds either. This restricted rotation around the C–N amide bond implies that the interconversion between the two conformers, *syn* & *anti*, of coumarin amides **5a–d** and thiazole 7 (Fig. 4), would be slow enough to manifest as distinct sets of signals in ^{1}HNMR and ^{13}C-NMR spectra.

The predominant conformer of coumarin and thiazole amides was anticipated to correspond to the more prominent signals, with the NH proton oriented in the *anti*-conformation to the C=O group, while the minor signals were expected to correspond to the *syn*-conformation (Fig. 4). This assignment stemmed from two primary reasons. Firstly, in the *syn*-conformer, the proximity between the two groups leads to repulsion due to steric interactions, particularly between bulky groups, thus favoring a shift in equilibrium towards the more stable *anti*-conformer. Secondly, the dipole moment across the C–N amide bond[26] results in a partial negative charge on one side of the bond and a partial positive charge on the opposite side. The region with partial negative charge possesses higher electron density at any given time, causing a shielding effect on surrounding protons.[27]

In the *anti*-conformation of thiazole amide 7, the amide NH proton resides directly on the positive end of the dipole. Consequently, the NH signal is expected to be less shielded,

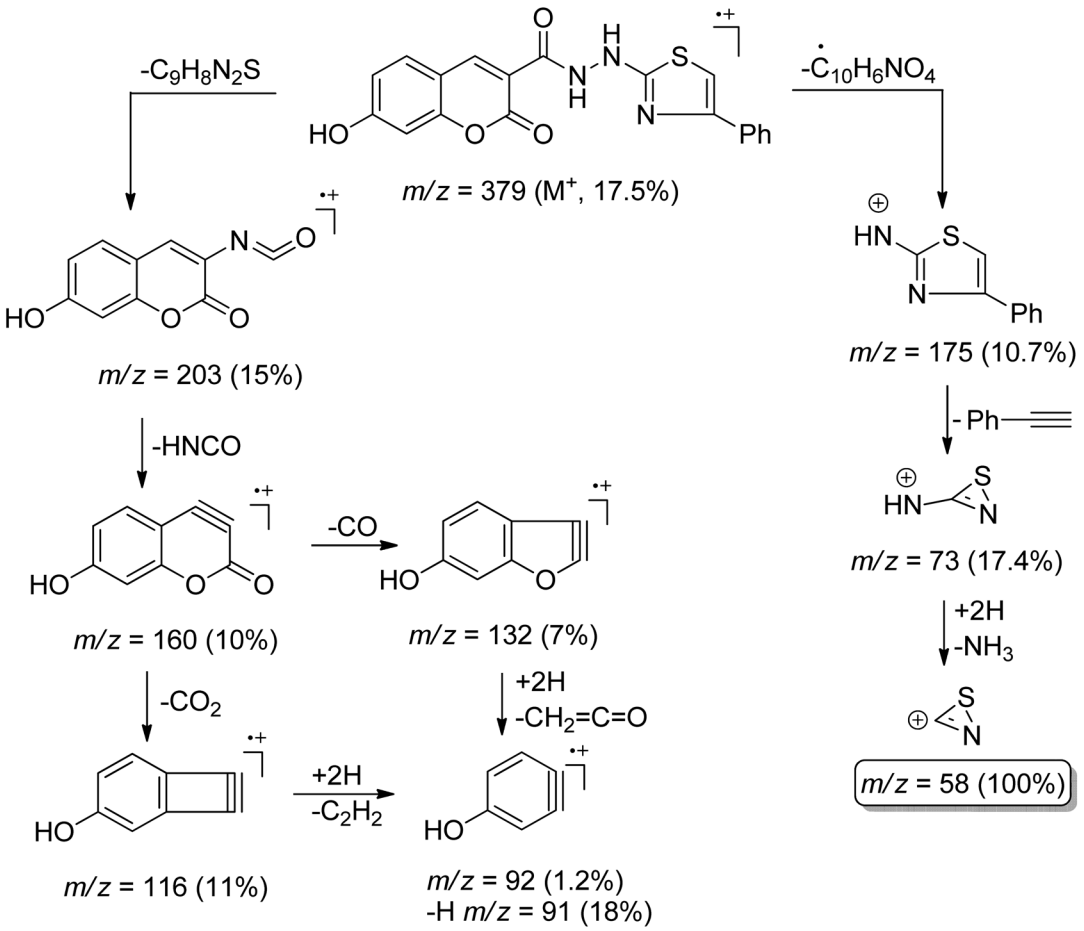

Scheme 3 Mass fragmentation pattern of compound **6c**.

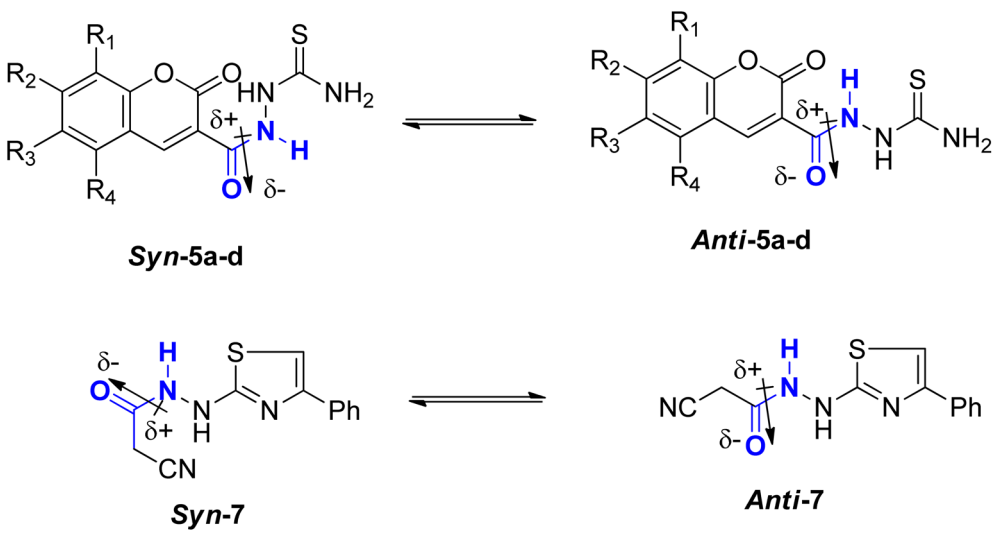

Fig. 4 *Syn* & *anti* conformers of coumarin amides **5a–d** & thiazole amide **7**.

appearing more downfield (at approximately 10.60 ppm) in the ^{1}HNMR spectrum. Conversely, in the *syn*-conformer of 7, the amide NH proton is distant from the positive end, resulting in the NH signal appearing more upfield (around 10.15 ppm) (Fig. 5). Similar assignments of *syn* and *anti*-conformations of amides using ^{1}HNMR spectra have been previously documented by LaPlanche and Rogers.[28]

On the contrary, the more intense signals in the ^{1}HNMR spectrum of coumarin amide **5a** were assigned to *syn*-conformer, and the less intense signals belonged to the minor

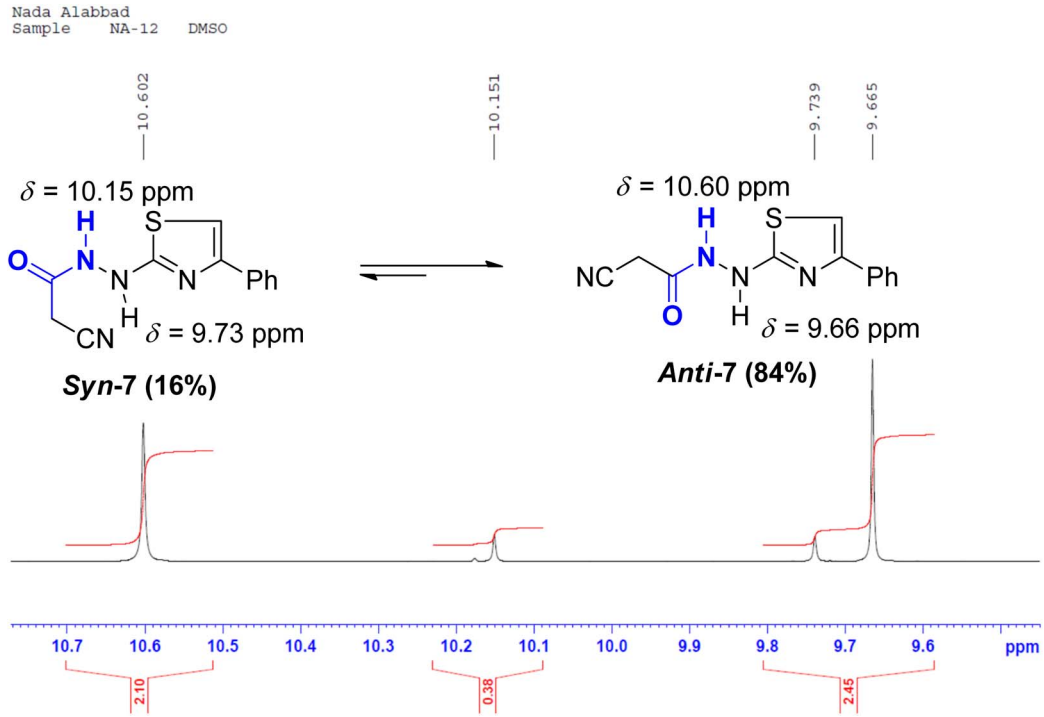

Fig. 5 A segment of ^{1}HNMR spectrum (500 MHz, DMSO-d_6) of thiazole *syn*-7 & *anti*-7.

isomer, *anti*-conformer. This assignment was consistent with the assumption of the deshielding effect of the dipole of a carbonyl group to the amidic NH proton in the *anti*-conformation. Fig. 6 shows that the amidic NH proton in the *anti*-isomer appears highly downfield at δ 13.04 ppm due to forming a possible intramolecular hydrogen bond with C=O of the coumarin ring.

While in the *syn*-isomer, this amidic proton displays at δ 11.54 ppm due to the shielding effect of the dipole of the carbonyl group around the C–N bond. Interestingly, the coumarin-H4 also appears at two different resonances. In the minor isomer, *anti*-conformer, this signal resonates slightly downfield at δ 9.48 ppm because of the magnetic anisotropic deshielding effect of the amidic carbonyl group. This finding also aligns with the research reported by Gribble and Bousquet.[29]

2.2. Antiproliferative evaluation and SAR study

The antiproliferative activity of the synthesized derivatives **5a–d**, **6a–d**, and 7 were evaluated against three human cancer cell lines in addition to normal cells using doxorubicin as a reference. The human cancerous cell lines were breast MCF-7, hepatocellular carcinoma HepG2, and colorectal HCT116 where their toxicity on normal cells was assessed using the somatic hybrid cells EA.hy926. The achieved results presented in Table 1 demonstrated the privilege of the open chain thioamides **5a–d** over their cyclized phenyl thiazole **6a–d** congeners against the three cancerous cell lines. The superiority of the hydroxyl substituted coumarins **5c** and **6c** owed to their ability to form extra H-bond with the hinge Asp145 as discussed later in the molecular docking section. The open chain **5c** showed an IC_{50} range of 4.5–7.5 μM while its thiazole congener **6c** demonstrated an IC_{50} range of 2.6–10.0 μM against the three tested cancerous cell lines. Nonetheless, **6c** exhibited a lower selectivity ratio than **5c** which showed normal EA.hy926 IC_{50} 8.4 μM compared to 26.6 μM of **5c**. Moreover, coumarin substitution with the electron-donating methoxy group **5b** and **6b** dropped the activity by 2–5 folds among the three cell lines. On the other hand, changing coumarin into phenyl coumarin **5d** improved its binding to CDK2 hydrophobic side chains, thus preserving the same activity as its hydroxy substituted congener **5c**. However, further cyclization of **5d** terminal thioamide into phenyl thiazole **6d** diminished its cytotoxicity probably because of its larger size that did not accommodate into the CDK2 hydrophobic pocket (see the docking section). In the same context, substituting the coumarin moiety with the cyano group in 7 managed to conserve the necessary binding pattern to the CDK2 hinge and hydrophobic pocket therefore, appreciated cytotoxicity was observed against the three cancerous cell lines (IC_{50} = 6.5–10.3 μM) with good selectivity ratio. A summary of the derivatives structure–activity relationship is presented in Fig. 7.

2.3. Molecular docking simulations

To assess the assumption of inhibiting CDK2, the synthesized derivatives were subjected to molecular docking simulations using the deposited crystal structure PDB ID: 3QTR, 1.85 Å.[30,31] The docking protocol was validated before commencing the actual simulation through self-docking of the co-crystallized ligand **X36** giving RMSD of 1.98 Å difference between the original and re-docked pose (ESI, Fig. S32†) using the open source DockRMSD.[32–34] Moreover, during derivatives preparation at the

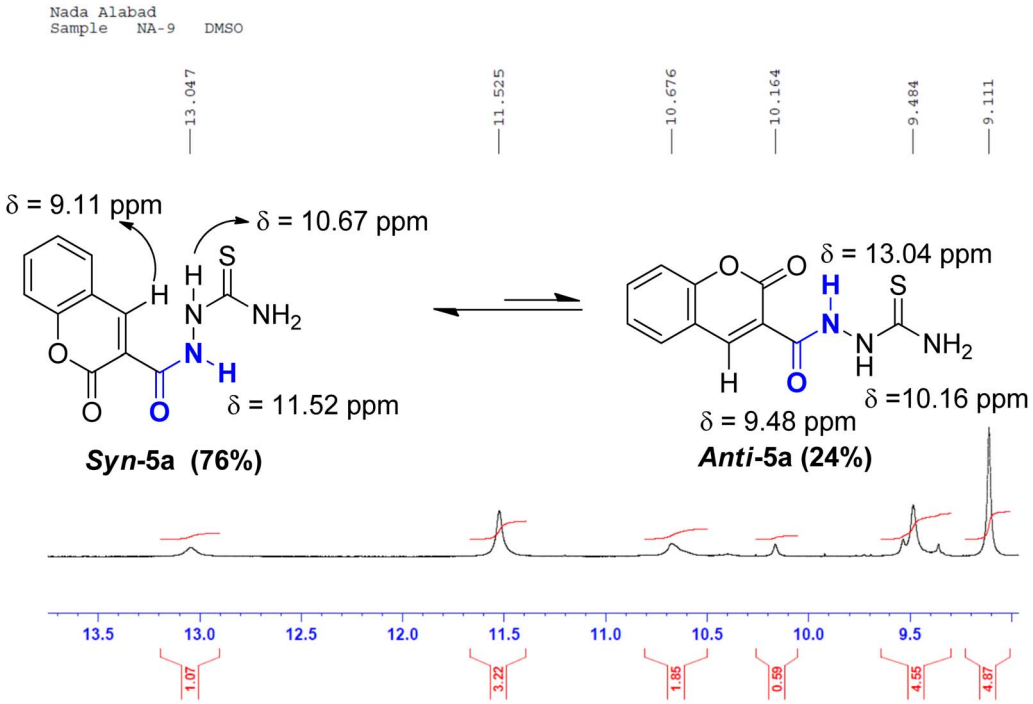

Fig. 6 A segment of ^{1}HNMR spectrum (500 MHz, DMSO-d_6) of coumarin *syn*-**5a** & *anti*-**5a**.

Table 1 The antiproliferative activity of **5a–d**, **6a–d**, and **7** after 72 h incubation in triplicates against doxorubicin as a positive reference

	MCF-7		HepG2		HCT116		EA.hy926	
Compound	IC_{50} (μM) ± SD		IC_{50} (μM) ± SD		IC_{50} (μM) ± SD		IC_{50} (μM) ± SD	
5a	28.6	0.3	17.7	0.1	15.2	0.7	20.0	0.7
5b	21.8	0.8	10.8	0.5	36.2	1.6	25.8	0.4
5c	4.5	0.4	5.4	0.3	7.5	0.3	26.6	0.3
5d	9.3	0.6	6.9	0.2	3.5	0.2	31.6	0.4
6a	72.9	0.8	36.5	1.8	82.5	0.5	31.9	1.2
6b	186.6	5.6	116.3	3.7	192.6	3.2	89.0	3.5
6c	10.0	1.0	2.6	0.1	3.5	0.1	8.4	0.3
6d	104.9	2.7	73.5	1.4	76.9	1.4	96.6	0.5
7	10.3	0.6	9.9	0.2	6.5	0.4	11.6	0.4
Doxorubicin	2.1	0.5	1.6	0.4	1.9	0.3	1.7	0.4

default docking forcefield MMFF94x, the carbohydrazide linkage was automatically changed into carbodiazene at the default temperature and pH. The obtained results (Table 2, Fig. 8–11) revealed that most of the interactions occurred in the ATP-binding site with residues Lys33, Leu83, Glu81 and the gatekeeper Phe80 suggesting a competitive mechanism of inhibition.[34–36] All tested derivatives except **6a** and **7** showed H-bond with the hinge Leu83 at an average distance of 2.50 Å through their diazene nitrogen or thioamide terminus resembling the purine ring of ATP. In a similar way, all derivatives expect **5a** and **5d** showed either H-bond or electrostatic attraction with the crucial Asp86 imitating **X36** (Table 2 and Fig. 8a). Furthermore, the coumarin scaffold was better oriented inside the hydrophobic pocket of CDK2 than the smaller benzoyl moiety of **X36** developing several π-sigma, π-alkyl and alkyl interactions with Ile10, Val18, Ala31, Leu134 and Ala144 (Table 2, Fig. 8–11).

It was observed that the most potent derivatives **5c**, **6c**, and **5d** showed better binding energy to CDK2 than **X36** demonstrating −9.40, −10.30, −10.20, and −9.20 kcal mol^{-1}, respectively (Table 2). Besides achieving better binding energy, cyclizing the thioamide terminus of **5c** into a thiazole ring in **6c** exposed two additional amide-π stacked interactions with His84 and Glu85 while preserving the H-bond with Leu83 and electrostatic attraction with Asp86 through its diazene linkage (Fig. 8b and d). These extra interactions further supported the orientation of **6c** inside the ATP-binding site better than **5c** and **X36** achieving double the antiproliferative effect of **5c** in the case of HepG2 and HCT116 (Fig. 8c and e). On the other hand, cyclizing the thioamide terminus of the benzo-coumarin **5d** into a thiazole ring in **6d** dropped the activity by 10 folds which was justified by their docking orientation. The smaller **5d** was better positioned inside the hinge region showing the usual H-bonds with leu83 and His84 in addition to its proper positioning in the neighboring hydrophobic side chain resulting in eight hydrophobic interactions with Ile18, Val18, Ala31, and leu134 (Fig. 9a and b). However, increasing the size of the compound by cyclizing the thioamide into a phenyl thiazole moiety exposed the large benzo-coumarin outside the hydrophobic pocket losing the aforementioned hydrophobic interactions except with Ile10 (Fig. 9c). Similarly, the cyclization of **5a** and **5b** into **6a** and **6b**, respectively resulted in abolishing their antiproliferative activity over the tested three cell lines probably by the same steric clashes with CDK2 (Fig. 10a–d).[19]

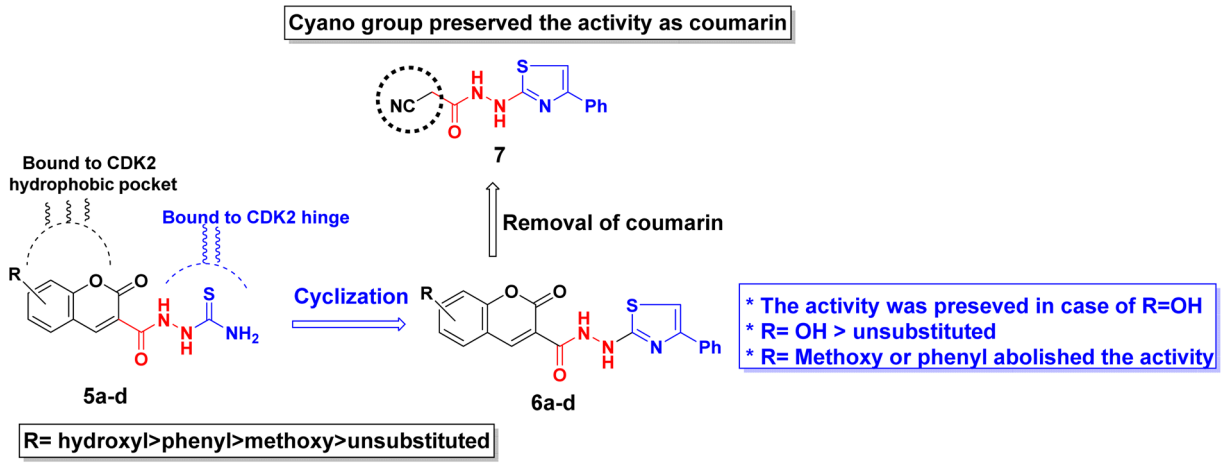

Fig. 7 Graphical presentation of the synthesized derivatives structure–activity relationship.

The ability of the phenyl thiazole moiety to imitate the coumarin binding pattern within the hydrophobic side chain was investigated in 7 where the coumarin was substituted with the open chain diazene acquiring a cyano group. Fig. 11a and b demonstrated the capability of the phenyl thiazole to form many hydrophobic interactions with the hydrophobic pocket residues in addition to the unique π–π interaction with the gatekeeper Phe80. Moreover, the cyano group formed a H-bond with the crucial Glu12 and Gly13 with an approximate distance of 2.96 Å which declared IC_{50} 10.3, 9.9, and 6.5 μM against MCF-7, HepG2, and HCT116, respectively.

2.4. Molecular dynamics simulation

The stability and binding affinity of compounds **5c** and **6c** were rigorously evaluated through molecular dynamics (MD) simulations extending for 100 nanoseconds. The analysis revealed that both derivatives maintained a commendable degree of stability throughout the simulation period. Notably, compound **5c** exhibited superior stability, as evidenced by its root mean square deviation (RMSD) profiles, with an average RMSD of 2.09 Å for compound **5c** compared to 3.27 Å for compound **6c** (Fig. 12A).

In the case of the unliganded protein, its structural integrity remained significantly stable, demonstrating minimal fluctuations throughout the simulation. This was quantitatively supported by an average RMSD of 2.12 Å and a root mean square fluctuation (RMSF) of 1.41 Å (Fig. 12B).

Moreover, the interaction energies of compounds **5c** and **6c** were evaluated, with mean values estimated at −65.38 kcal mol^{-1} and −52.44 kcal mol^{-1}, respectively, as shown in Fig. 13. Additionally, the binding free energies of these compounds, calculated using the MM-PBSA method, were determined to be −13.31 kcal mol^{-1} for compound **5c** and −6.20 kcal mol^{-1} for compound **6c**, indicating their potential binding affinities (Table 3).

The investigation also highlighted the formation of stable hydrophilic contacts, especially hydrogen bonds, with both compounds forming between 1 and 3 hydrogen bonds during the simulation (ESI, Fig. S35†).

In summation, the findings suggested that compounds **5c** and **6c** exhibited satisfactory to moderate levels of binding stability and affinity within the active site of the target CDK2. This observation pointed towards their potential as CDK2 inhibitors, underlining their significance in further drug development efforts.

2.5. Physicochemical and pharmacokinetics prediction

The physicochemical descriptors and pharmacokinetics properties of the synthesized derivatives were calculated using the SwissADME web tool from the Swiss Institute of Bioinformatics (SIB).[37,38] The obtained prediction was summarized in ESI, Table S1† demonstrated compliance with Lipinski's rule of five giving a bioavailability score of 0.55.[39,40] The predicted values of molecular weight, rotatable bonds, H-bond donor, and acceptors were within the acceptable limit of being less than 500 g per mole, 10, 5, and 10, respectively. Moreover, the topological polar surface area of the derivatives was less than 170 $Å^2$ complying with Veber's rule of bioavailability which translated into high GI absorption except for the relatively more polar **5c**.[41–43] In addition, the in-house log $P_{o/w}$ evaluation showed values less than 5 among all tested derivatives which accounted for their promising bioavailability.[44,45] They were expected to not cross the blood–brain barrier and not be affected by the efflux pump P-glycoprotein.[46,47] However, some could affect the level of cytochrome P-450 isoenzymes which needs more cautious during further implementation.

3. Experimental section

3.1. Synthesis and spectroscopic characterization

3.1.1. Synthesis of 1-cyanoacetylthiosemicarbazide 3. In a 250 mL conical flask, thiosemicarbazide **1** (20 mmol, 1.82 g) and **2** (20 mmol, 3.26 g) were dissolved in ethanoic acid (30 mL) and then warmed at 60 °C with stirring for 3 h. The product achieved was gathered by filtration and recrystallized from aqueous ethyl alcohol. White powder; yield 85%; MP = 189–191 °C; IR (KBr) ν_{max}/cm^{-1} = 3415, 3270 (NH_2), 3210, 3137 (NH), 2961, 2929 (C–H sp^3), 2257 (C≡N), 1688 (C=O), 1294 (C=S); ^{1}H-NMR (850 MHz, DMSO-d_6): δ_{ppm} = 3.63 (s, 2H, CH_2), 7.68 (s,

Table 2 Molecular docking simulation results of the co-crystallized ligand **X36** and derivatives **5a–d**, **6a–d**, and **7** using PDB ID: 3QTR, 1.85 Å (HPO: hydrophobic)

Compound	Binding energy in kcal mol^{-1}	Interaction type	Interacting residues	Distance in Å	H-bond angle
X36	−9.20	H-donor	Asp86	2.41	121.30
		HPO amide-π	A: GLN85: C,O; ASP86: N	5.04	
		HPO π-alkyl	ILe10	5.34	
		HPO π-alkyl	Va18	4.66	
		HPO π-alkyl	Va18	5.47	
		HPO π-alkyl	Ala31	4.60	
		HPO π -alkyl	Val64	5.21	
		HPO π-alkyl	Leu134	5.30	
		HPO π-alkyl	Ala144	3.88	
		HPO π-alkyl	Ile10	4.12	
5a	−8.50	H-acceptor	Leu83	2.00	158.83
		H-donor	Leu83	2.49	128.20
		Electrostatic π-cation	Phe82	4.27	
		HPO π-sigma	Val18	2.55	
		π-Sulfur	Phe82	5.24	
		HPO π-alkyl	Ile10	5.21	
		HPO π-alkyl	Val18	5.12	
		HPO π-alkyl	Ala31	4.29	
		HPO π-alkyl	Leu134	4.30	
		HPO π-alkyl	Ala31	4.82	
		HPO π-alkyl	Leu134	5.44	
5b	−8.90	H-donor	Asp86	2.28	1.53.293
		Electrostatic	Asp86	3.76	
		H-donor	Leu83	2.52	108.32
		HPO π-sigma	Phe80	3.61	
		HPO alkyl	Ala144	3.41	
		HPO alkyl	Val64	4.11	
		HPO π-alkyl	Ile10	5.33	
		HPO π-alkyl	Val18	4.28	
		HPO π-alkyl	Ala31	4.98	
		HPO π-alkyl	Leu134	4.86	
		HPO π-alkyl	Val18	3.81	
5c	−9.80	Electrostatic	Asp86	4.11	
		Electrostatic	Asp86	3.97	
		H-donor	Leu83	2.36	166.32
		H-donor	Asp145	2.38	118.21
		HPO π-sigma	Val18	2.80	
		HPO π-alkyl	Ile10	5.43	
		HPO π-alkyl	Ala31	4.62	
		HPO π-alkyl	Leu134	4.93	
		HPO π-alkyl	Val18	4.70	
		HPO π-alkyl	Ala31	4.72	
		HPO π-alkyl	Ala144	4.41	
5d	−10.20	H-acceptor	Leu83	1.92	162.22
		H-donor	Leu83	2.87	121.27
		H-donor	His84	2.43	150.70
		Electrostatic π-cation	Phe82	4.29	
		HPO π-sigma	Val18	2.50	
		HPO π-alkyl	Ile10	5.25	
		HPO π-alkyl	Val18	5.11	
		HPO π-alkyl	Ala31	4.16	
		HPO π-alkyl	Leu134	4.34	
		HPO π-alkyl	Ala31	4.65	
		HPO π-alkyl	Leu134	5.50	
		HPO π-alkyl	Val18	3.76	
6a	−7.40	H-donor	Asp86	2.53	156.72
		Electrostatic	Asp86	4.13	
		H-donor	Ile10	2.26	115.92
		HPO amide-π	A: GLN85: C, O; ASP86: N	5.03	
		HPO π-alkyl	Ile10	4.30	
		HPO π-alkyl	Val18	3.65	

Table 2 (*Contd.*)

Compound	Binding energy in kcal mol^{-1}	Interaction type	Interacting residues	Distance in Å	H-bond angle
		HPO π-alkyl	Val18	3.95	
		HPO π-alkyl	Ala31	5.30	
		HPO π-alkyl	Lys33	4.97	
6b	−7.50	Electrostatic	Asp86	4.74	
		Electrostatic	Asp86	5.03	
		H-donor	Leu83	2.68	120.30
		Electrostatic	Leu298	4.94	
		HPO alkyl	Val18	3.76	
		HPO alkyl	Lys33	4.06	
		HPO π-alkyl	Ala31	4.76	
6c	−10.30	Electrostatic	Asp86	4.90	
		Electrostatic	Asp86	5.07	
		H-acceptor	Lys89	3.09	126.25
		H-donor	Leu83	2.48	127.87
		H-donor	Asp145	2.50	109.37
		H-acceptor	Asp145	2.70	120.02
		HPO π-sigma	Val18	2.80	
		HPO π-sigma	Gln85	2.93	
		HPO amide-π	A: HIS84: C, O; GLN85: N amide	4.01	
		HPO π-alkyl	Ala31	4.35	
		HPO π-alkyl	Leu134	4.88	
		HPO π-alkyl	Ala144	5.26	
		HPO π-alkyl	Val18	4.87	
		HPO π-alkyl	Ala31	4.71	
		HPO π-alkyl	Ala144	4.33	
6d	−7.60	H-acceptor	Leu83	2.95	140.57
		H-acceptor	Asp86	2.70	110.25
		Electrostatic	Asp145	3.49	
		HPO π-sigma	Val18	2.66	
		HPO π-alkyl	Ile10	4.71	
		HPO π-alkyl	Ala31	4.92	
		HPO π-alkyl	Val18	5.38	
7	−8.30	H-donor	Asp86	2.10	170.08
		Electrostatic	Asp86	4.00	
		H-acceptor	Glu12	2.96	100.95
		H-acceptor	Lys89	2.65	171.64
		H-acceptor	Gly13	2.97	142.60
		HPO π–π	Phe80	5.14	
		HPO π-alkyl	Ile10	5.03	
		HPO π-alkyl	Leu134	4.65	
		HPO π-alkyl	Val18	5.18	
		HPO π-alkyl	Ala31	4.65	
		HPO π-alkyl	Leu134	5.07	
		HPO π-alkyl	Ala144	3.96	

1H, NH^a-4); 7.99 (s, 1H, NH^b-4), 9.35 (s, 1H, NH-2), 10.14 (s, 1H, amidic-NH); ^{13}C-NMR (212.5 MHz, DMSO-d_6): δ_{ppm} = 24.73 (CH_2), 116.18 (CN), 162.64 (C=O), 182.32 (C=S); anal. calcd. For $C_4H_6N_4OS$ (158.18): C, 30.37; H, 3.82; N, 35.42%; found: C, 30.36; H, 3.84; N, 35.40%.

3.1.2. General procedure for creation of coumarin derivatives (5a–d). To a solution of **3** (6 mmol, 0.95 g) and substituted 2-hydroxybenzaldehydes **4a–d** (6 mmol) in 20 mL ethyl alcohol, 0.1 mL of piperidine was added. The content was heated for 4–9 h, and TLC checked the reaction progress. The reaction was quenched by adding ice-cold water (20 mL) having (0.1 mL) of conc HCl. The formed adduct was gathered by filtration and purified by crystallization from EtOH.

*3.1.2.1. 2-(2-Oxo-2H-chromene-3-carbonyl) hydrazine-1-carbothioamide (**5a**).* This substance was obtained from **3** and salicylaldehyde (6 mmol, 0.73 g) by heating for 4 h. Orange powder; yield: 40%; MP = 200–202 °C; IR (KBr) ν_{max}/cm^{-1} = 3404, 3253 (NH_2) 3282, 3098 (NH), 2964 (CH-sp^3), 1721 (C=O), 1674 (amidic C=O), 1273 (C=S); ^{1}H-NMR (850 MHz, DMSO-d_6): δ_{ppm} = 7.24 (d, J = 8.5 Hz, 2H, coumarin-$H_{5,8}$)**, 7.27 (t, J = 7.65 Hz, 1H, coumarin-H_6)**, 7.41–8.42 (m, 9H, coumarin-$H_{5,6,7,8}$ + NH_2), 9.11 (s, 1H, coumarin-H_4)**, 9.48 (s, 1H, coumarin-H_4)*, 10.16 (s, 1H, NH)*, 10.67 (s, 1H, NH)**; 11.52 (s, 1H, amidic-NH)**, 13.04 (s, 1H, amidic-NH)*; ^{13}C-NMR (212.5 MHz, DMSO-d_6): δ_{ppm} = 115.50 (coumarin-C_3), 116.71 (coumarin-C_8)*, 116.80 (coumarin-C_8)**, 118.75 (coumarin-

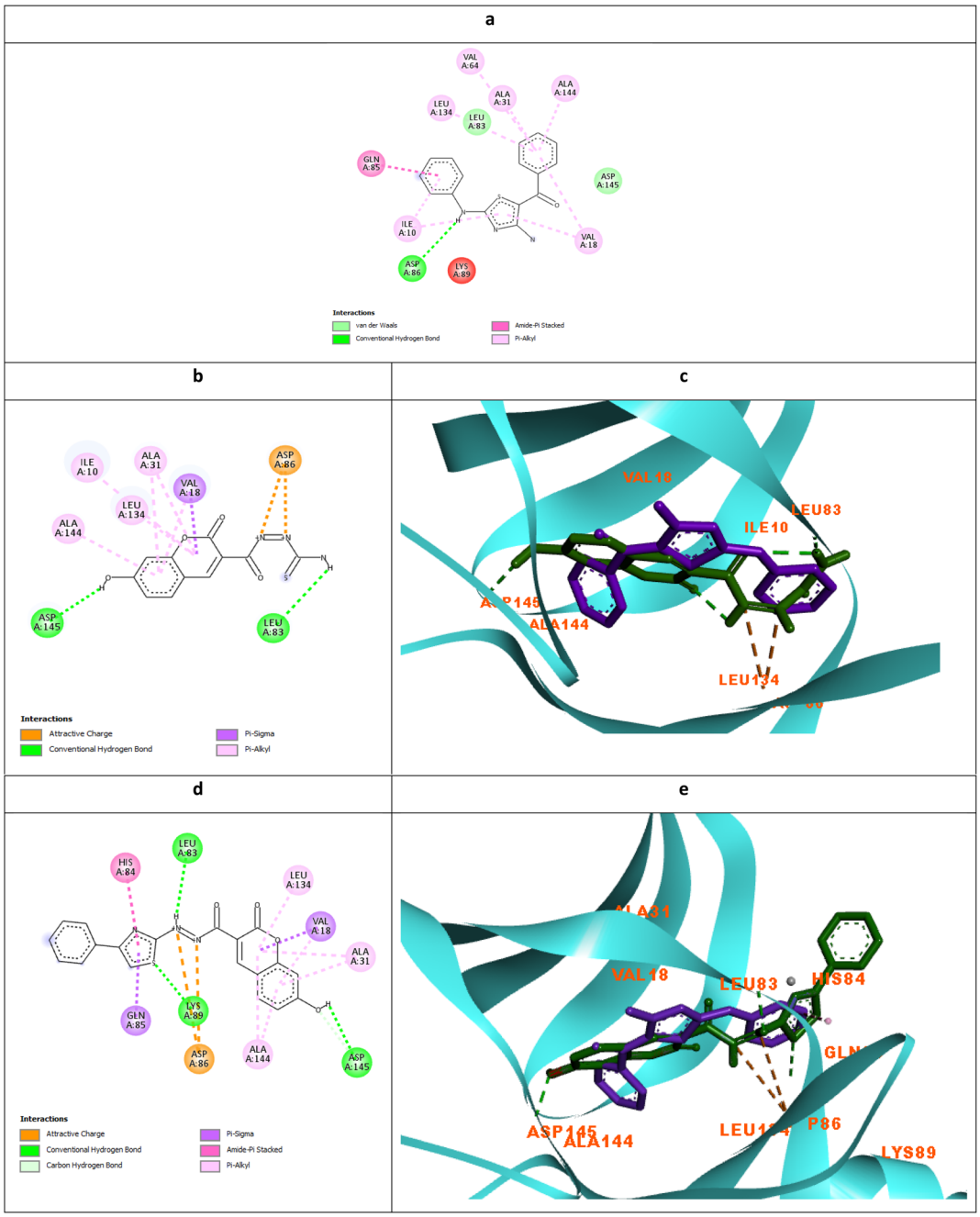

Fig. 8 Molecular docking simulations of the co-crystallized ligand **X36** (a), **5c** (b and c) and **6c** (d and e) using PDB ID: 3QTR, 1.85 Å. The evaluated derivatives appeared as a green stick model relative to the magenta-colored **X36** showing the interaction bonds as dotted lines.

C_{4a}), 119.41 (coumarin-C_4)*, 119.90 (coumarin-C_4)**, 124.70 (coumarin-C_6)**, 125.76 (coumarin-C_6)*, 130.37 (coumarin-C_5)**, 130.74 (coumarin-C_5)*, 133.62 (coumarin-C_7)**, 134.82 (coumarin-C_7)*, 153.82 (coumarin-C_{8a})**, 154.33 (coumarin-C_{8a})*, 158.30 (amidic-C=O), 161.97 (coumarin-C=O), 182.12 (C=S); MS *m*/*z* (%): 263 (M^+, 39.82), 234 (100), 171 (31.65), 112 (27.86), 60 (26.93); anal. calcd. For $C_{11}H_9N_3O_3S$ (263.27): C, 50.18; H, 3.45; N, 15.96%; found: C, 50.15; H, 3.47; N, 15.95%.

Signals are ascribed to * *anti* and ** to *syn* stereoisomers in this spectrum.

*3.1.2.2. 2-(8-Methoxy-2-oxo-2H-chromene-3-carbonyl) hydrazine-1-carbo-thioamide (**5b**).* This substance was obtained from **3** and *o*-vanillin (6 mmol, 0.91 g) by heating for 8 h. Orange powder; yield 70%; MP = 160–162 °C; IR (KBr) ν_{max}/cm^{-1} = 3404, 3341 (NH_2), 3282, 3177 (NH), 2968 (CH-sp^3), 1704 (C=O), 1651 (amidic C=O), 1273 (C=S), ^{1}H-NMR (850 MHz, DMSO-d_6): δ_{ppm} = 3.80 (s, 3H, OCH_3), 7.00 (s, 2H, NH_2); 7.34–7.42 (m, 2H, coumarin-$H_{6,7}$); 7.66 (d, J = 7.5 Hz, 1H, coumarin-H_5); 8.58 (s, 1H, coumarin-H_4)*, 8.89 (s, 1H, coumarin-H_4)**, 9.96 (s, 1H, NH), 13.47 (s, 1H, amidic-NH)*, 13.84 (s, 1H, amidic-NH)**; ^{13}C-NMR (212.5 MHz, DMSO-d_6): δ_{ppm} = 56.62 (CH_3)**, 56.70

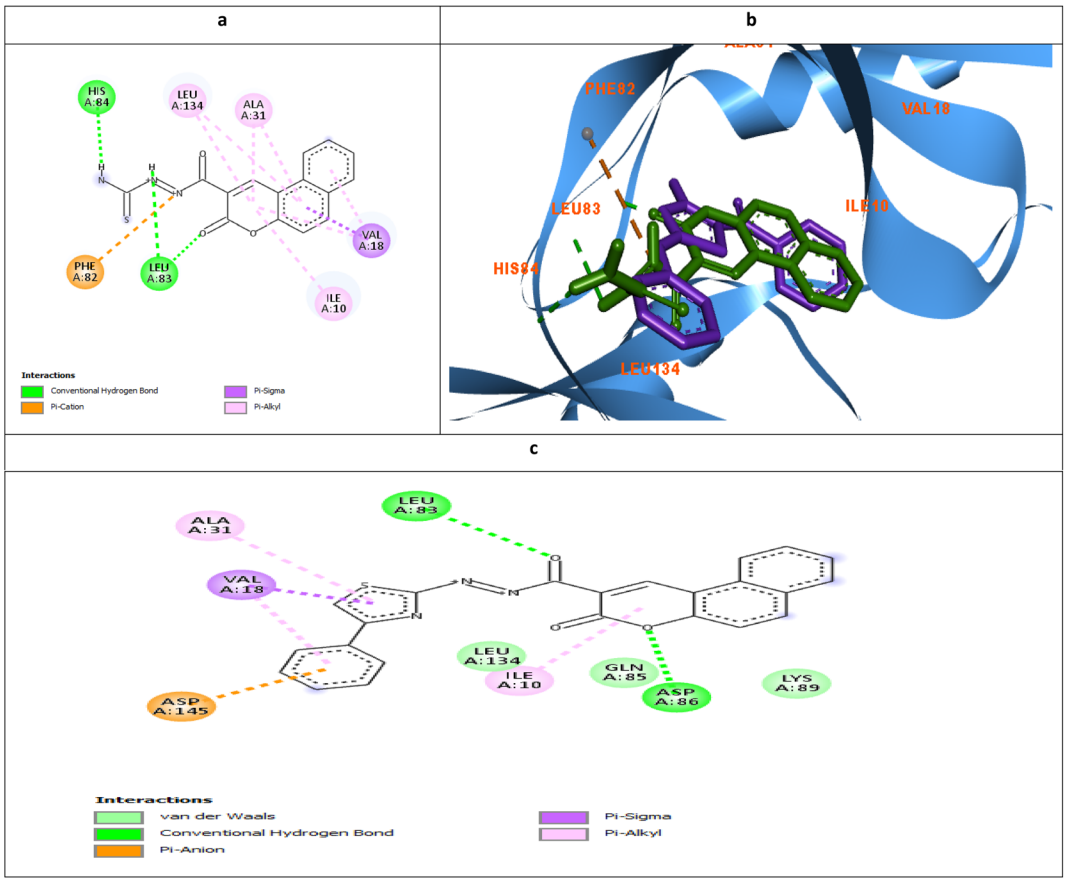

Fig. 9 Molecular docking simulations of **5d** (a and b) and **6d** (c) using PDB ID: 3QTR, 1.85 Å. The evaluated derivatives appeared as a green stick model relative to the magenta-colored **X36** showing the interaction bonds as dotted lines.

(CH_3)*, 114.21 (coumarin-C_3), 115.43 (coumarin-C_7)**, 116.19 (coumarin-C_7)*, 119.21 (coumarin-C_4)**, 119.86 (coumarin-C_4)*, 120.79 (coumarin-C_5)*, 121.00 (coumarin-C_5)**, 125.41 (coumarin-C_{4a})*, 125.59 (coumarin-C_{4a})**, 143.02 (coumarin-C_6)*, 143.28 (coumarin-C_6)**, 144.07 (coumarin-C_{8a})*, 144.35 (coumarin-C_{8a})**, 146.69 (coumarin-C_8)**, 146.85 (coumarin-C_8)*, 157.36 (amidic C=O)*, 160.02 (amidic C=O)**, 167.32 (coumarin C=O), 177.03 (C=S); MS *m/z* (%): 293 (M^+, 17.47), 263 (30.77), 174 (12.89), 146 (14.96), 119 (17.09), 92 (43.03), 44 (100); anal. calcd. For $C_{12}H_{11}N_3O_4S$ (293.30) C, 49.14; H, 3.78; N, 14.33%; found: C, 49.11; H, 3.77; N, 14.35%.

Signals are ascribed to * *anti* and ** to *syn* stereoisomers in this spectrum.

*3.1.2.3. 2-(7-Hydroxy-2-oxo-2H-chromene-3-carbonyl) hydrazine-1-carbo-thioamide (**5c**).* This substance was obtained from **3** and 2,4-dihydroxybenzaldehyde (6 mmol, 0.83 g) by heating for 8 h. Yellow powder; yield: 56%; MP = 292–294 °C; IR (KBr) ν_{max}/cm^{-1} = 3269, 3214 (2NH), 3108, 3066 (C–H sp^2), 1714 (coumarin C=O), 1683 (amidic C=O), 1277 (C=S); ^{1}H-NMR (850 MHz, DMSO-d_6): δ_{ppm} = 4.80 (s, 1H, coumarin-H_8), 6.92 (d, J = 8.5 Hz, 1H, coumarin-H_6), 7.20 (s, 2H, NH_2), 7.67 (d, J = 8.5 Hz, 1H, coumarin-H_5), 8.20 (s, 1H, NH), 8.59 (s, 1H, coumarin-H_4), 10.83 (s, 1H, OH), 13.86 (s, 1H, amidic NH); ^{13}C-NMR (212.5 MHz, DMSO-d_6): δ_{ppm} = 105.50 (coumarin-C_8), 113.30 (coumarin-C_3), 136.10 (coumarin-C_5), 156.50 (coumarin-C=O), 168.43 (amidic-C=O), 181.12 (C=S); anal. calcd. For $C_{11}H_9N_3O_4S$ (279.27): C, 47.31; H, 3.25; N, 15.05%; found: C, 47.33; H, 3.27; N, 15.03%.

*3.1.2.4. 2-(3-Oxo-3H-benzo[f]chromene-2-carbonyl)hydrazine-1-carbothio-amide (**5d**).* This substance was obtained from **3** and 2-hydroxy-1-naphthaldehyde (6 mmol, 1.03 g) by heating for 8 h. Orange powder; yield: 78%; MP = 186–187 °C; IR (KBr) ν_{max}/cm^{-1} = 3312, 3259 (NH_2), 3163 (NH), 2980, 2970 (CH sp^3), 1716 (coumarin C=O), 1675 (amidic C=O), 1273 (C=S); ^{1}H-NMR (850 MHz, DMSO-d_6): δ_{ppm} = 7.20 (s, 2H, NH_2), 7.62 (t, J = 6.8 Hz, 1H, coumarin-H_8), 7.76 (t, J = 7.65 Hz, 1H, coumarin-H_9), 8.15 (d, J = 8.5 Hz, 2H, coumarin-H_{10}); 8.27 (d, J = 8.5 Hz, 1H, coumarin-H_7), 8.68 (d, J = 8.5 Hz, 1H, coumarin-H_8), 9.35 (s, 1H, coumarin-H_4), 9.76 (s, 1H, NH), 10.70 (s, 1H, amidic-NH); ^{13}C-NMR (212.5 MHz, DMSO-d_6): δ_{ppm} = 113.07 (coumarin-C_3), 116.97 (coumarin-C_{4a}), 118.01 (coumarin-C_{10}), 122.89 (coumarin-C_5), 126.07 (coumarin-C_7), 127.15 (coumarin-C_6), 128.03 (coumarin-C_8), 129.48 (coumarin-C_{8a}), 135.04 (coumarin-C_{5a}), 136.57 (coumarin-C_9), 155.11 (coumarin C_4), 159.75 (amidic C=O), 163.15 (coumarin-C=O), 183.12 (C=S); anal. calcd. For $C_{15}H_{11}N_3O_3S$ (313.33): C, 57.50; H, 3.54; N, 13.41%; found: C, 57.53; H, 3.52; N, 13.43%.

3.1.3. General procedure for production of coumarin-thiazole hybrids (6a–d). A solution of phenacyl bromide (4 mmol, 0.78 g) in ethanol (30 mL) was added (4 mmol) of

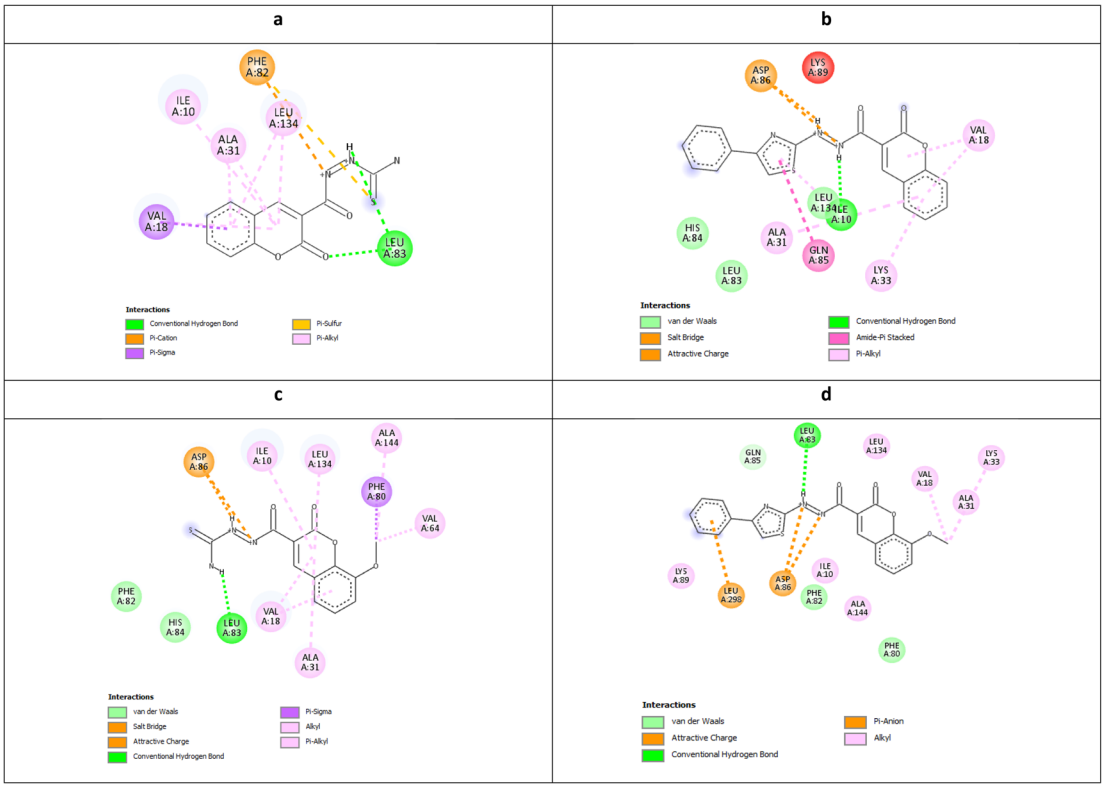

Fig. 10 Molecular docking simulations of **5a** (a), **6a** (b), **5b** (c), and **6b** (d) using PDB ID: 3QTR, 1.85 Å.

appropriate compounds **5a–d** and 0.1 mL of triethylamine. The solution was allowed to reflux for 10 h. After cooling to room temperature, the solution was poured portion-wise onto ice water (30 mL) containing 0.1 mL of HCL while stirring. The adducts formed were picked up and purified by boiling with a suitable solvent.

*3.1.3.1. 2-Oxo-N′-(4-phenylthiazol-2-yl)-2H-chromene-3-carbohydrazide (**6a**).* This substance was obtained from heating coumarin **5a** (4 mmol, 1.05 g) and phenacyl bromide (4 mmol, 0.78 g) for 6 h and was crystallized from EtOH. Orange powder; yield: 61%; MP = 205–207 °C; IR (KBr) ν_{max}/cm^{-1} = 3291, 3113 (NH), 3078 (CH-sp^2), 2980, 2971 (CH-sp^3), 1715 (coumarin-C=O), 1682 (amidic C=O); ^{1}H-NMR (850 MHz, DMSO-d$_6$): δ_{ppm} = 7.29 (t, J = 6.8 Hz, 1H, Ar-H$_4$), 7.30 (s, 1H, thiazole-H$_5$), 7.40 (t, J = 7.65 Hz, 2H, Ar-H$_{3,5}$), 7.46 (t, J = 7.65 Hz, 1H, coumarin-H$_6$), 7.53 (d, J = 8.5 Hz, 1H, coumarin-H$_8$), 7.77 (t, J = 7.65 Hz, 1H, coumarin-H$_7$), 7.85 (d, J = 7.65 Hz, 2H, Ar-H$_{2,6}$); 8.00 (d, J = 7.65 Hz, 1H, coumarin-H$_5$), 8.85 (s, 1H, coumarin-H$_4$), 9.92 (s, 1H, thiazole-NH), 10.68 (s, 1H, amidic-NH); ^{13}C-NMR (212.5 MHz, DMSO-d$_6$): δ_{ppm} = 103.99 (thiazole-C$_5$), 116.69 (coumarin-C$_3$), 118.72 (coumarin-C$_8$), 119.39 (coumarin-C$_{4a}$), 125.63 (coumarin-C$_{4,6}$), 126.06 (Ar-C$_{2,6}$), 128.02 (coumarin-C$_5$), 129.06

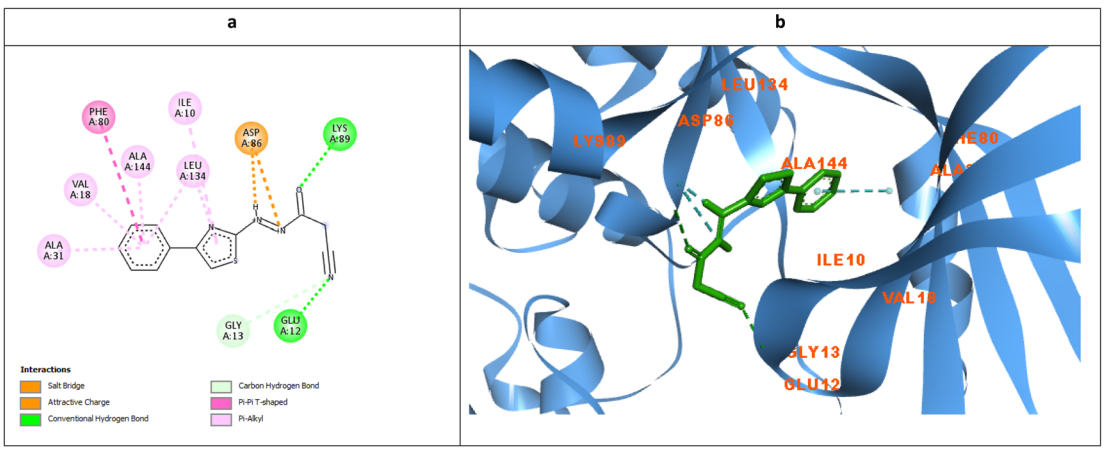

Fig. 11 Molecular docking simulations of **7** (a and b) using PDB ID: 3QTR, 1.85 Å. The evaluated derivatives appeared as a green stick model showing the interaction bonds as dotted lines.

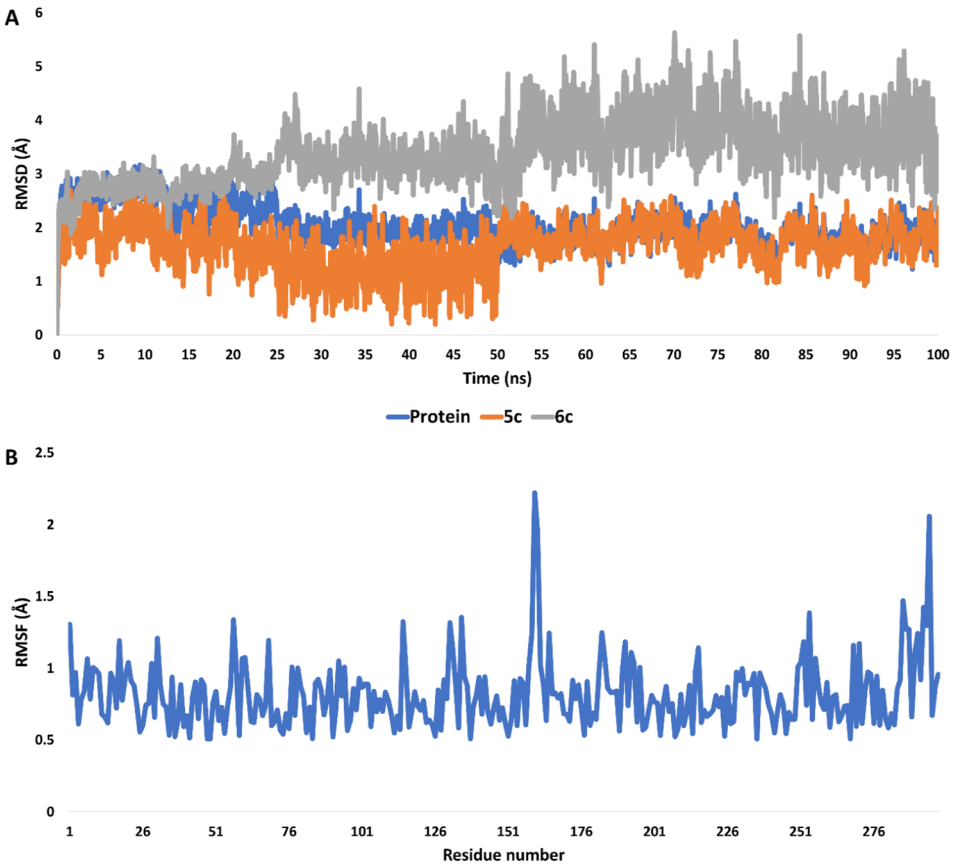

Fig. 12 (A) RMSDs of compounds **5c** and **6c** inside the active site of CDK2 (PDB ID: 3QTR) along with that of the unliganded protein throughout 100 ns-long MD simulation. (B) RMSF profile of the unliganded CDK2 throughout 100 ns-long MD simulation.

(Ar-$C_{3,5}$), 130.79 (coumarin-C_7), 134.87 (Ar-C_4), 148.26 (Ar-C_1), 150.94 (thiazole-C_4), 154.47 (coumarin-C_{8a}), 159.91 (coumarin-C=O), 161.98 (amidic-C=O), 171.40 (thiazole-C_2); MS *m*/*z* (%): 363 (M^+, 10.88), 324 (38.92), 227 (10.08), 196 (18.17), 181 (6.75), 136 (19.04), 110 (9.88), 82 (26.88), 69 (100), 58 (37.24), 44 (18.43).

*3.1.3.2 8-Methoxy-2-oxo-N′-(4-phenylthiazol-2-yl)-2H-chromene-3-carbo-hydrazide (**6b**).* This substance was obtained from heating coumarin **5b** (4 mmol, 1.17 g) and phenacyl bromide (4 mmol, 0.78 g) for 7 h and was crystallized from a mixture of EtOH and $CHCl_3$. Brown powder; yield: 69%; MP = 229–231 °C; IR (KBr) ν_{max}/cm^{-1} = 3291, 3265 (NH), 3113, 3055 (=C–H sp^2), 2968 (–C–H sp^3); 1682 (coumarin C=O), 1635 (amidic C=O), ^{1}H-NMR (500 MHz, DMSO-d_6): δ_{ppm} = 2.51 (s, 3H, OCH_3), 6.83 (s, 1H, thiazole-H_5), 7.37–7.47 (m, 4H, Ar-$H_{3,4,5}$ + coumarin-H_6), 7.84–7.91 (m, 2H, coumarin-$H_{5,7}$), 7.95 (s, 1H, NH), 7.97 (d, *J* = 5 Hz, 2H, Ar-$H_{2,6}$)*, 8.04 (d, *J* = 5 Hz, 2H, Ar-$H_{2,6}$)**, 8.19 (s, 2H, coumarin-H_4 + amidic-NH); ^{13}C-NMR (125 MHz, DMSO-d_6): δ_{ppm} = 55.54 (OCH_3), 109.41 (thiazole-C_5), 110.48 (coumarin-C_3), 112.56 (coumarin-C_{4a}), 125.61 (coumarin-$C_{4,7}$), 126.45 (Ar-$C_{2,6}$), 128.82 (coumarin-C_6), 128.96 (coumarin-C_5), 129.28 (Ar-$CH_{3,5}$), 129.43 (Ar-CH_4), 133.59 (Ar-C_1)*, 133.84 (Ar-C_1)**, 134.41 (coumarin-C_{8a}), 139.49 (coumarin-C_8), 142.72 (Thiazole-C_4), 151.89 (coumarin C=O)**, 152.16 (coumarin-C=O)*, 160.61 (amidic C=O)*, 160.97 (amidic C=O)**, 161.69 (thiazole-C_2)**, 162.84 (thiazole-C_2)*; MS *m*/*z* (%): 393 (M^+, 22.67), 317 (3.21), 234 (12.13), 204 (3.12), 174 (4.67), 132 (7.11), 119 (37.94), 90 (4.86), 66 (24.64), 40 (100).

Signals are ascribed to * *anti* and ** to *syn* stereoisomers in this spectrum.

*3.1.3.3. 7-Hydroxy-2-oxo-N′-(4-phenylthiazol-2-yl)-2H-chromene-3-carbohy-drazide (**6c**).* This substance was obtained from heating coumarin **5c** (4 mmol, 1.12 g) and phenacyl bromide (4 mmol, 0.78 g) for 10 h and was crystallized from EtOH. White powder; yield: 31%; MP = 258–260 °C; IR (KBr) ν_{max}/cm^{-1} = 3241 (NH), 3065 (C–H sp^2), 2973, 2925 (C–H sp^3), 1710 (coumarin C=O), 1682 (amidic C=O); ^{1}H-NMR (850 MHz, DMSO-d_6): δ_{ppm} = 4.85 (s, 2H, NH + coumarin-H_8), 6.80 (s, 1H, thiazole-H_5), 6.86 (d, *J* = 8.5 Hz, 1H, coumarin-H_6), 7.57 (t, *J* = 7.65 Hz, 2H, Ar-$H_{3,5}$), 7.69 (t, *J* = 7.65 Hz, 1H, Ar-H_4), 7.72 (d, *J* = 8.5 Hz, 1H, coumarin-H_5), 8.05 (d, *J* = 7.65 Hz, 2H, Ar-$H_{2,6}$), 8.63 (s, 1H, coumarin-H_4), 10.97 (s, 1H, OH), 13.93 (s, 1H, amidic NH); ^{13}C-NMR (212.5 MHz, DMSO-d_6): δ_{ppm} = 102.52 (coumarin-C_8), 111.62 (thiazole-C_5), 115.32 (coumarin-C_3), 128.88 (Ar-$C_{2,6}$ + coumarin-$C_{4a,4}$), 129.29 (Ar-$C_{3,5}$ + coumarin-$C_{6,7,8a}$), 131.71 (Ar-C_4), 134.06 (Ar-C_1), 136.15 (coumarin-C_5), 143.57 (thiazole-C_4), 156.03 (coumarin-C=O), 162.52 (amidic-C=O), 168.43 (thiazole-C_2); MS *m*/*z* (%): 379 (M^+, 17.57), 203 (15), 175 (10.7), 160 (10), 132 (7%), 116 (11%), 92 (1.2), 91 (18), 73 (17.4), 58 (100).

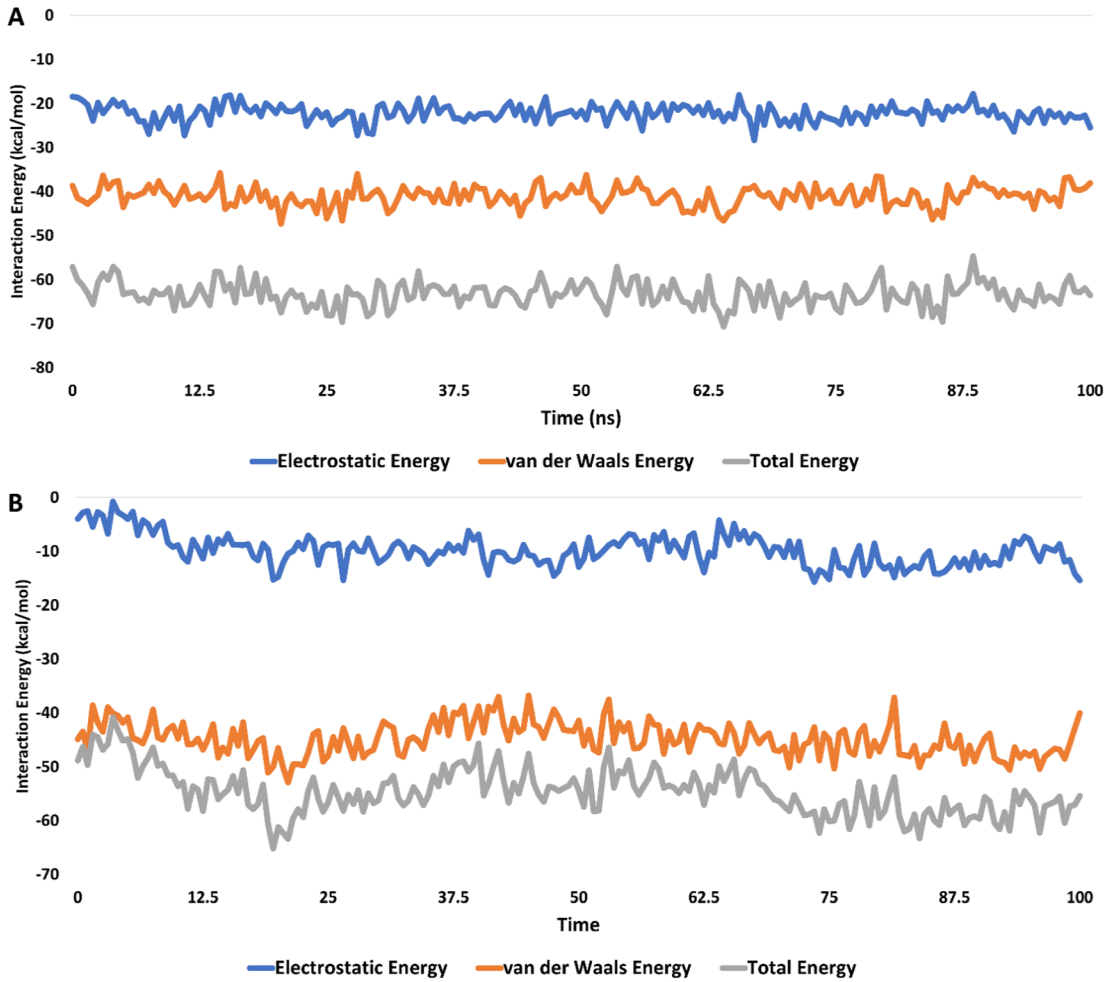

Fig. 13 The interaction energies of compounds **5c** (A) and **6c** (B) inside the active site of CDK2 (PDB ID: 3QTR) for 100 ns-long MD simulation.

Table 3 The binding free energies ($\Delta G_{binding}$) of **5c** and **6c** in complex with the CDK2 (PDB ID: 3QTR) were calculated in kcal mol^{-1}

Energy component	5c	6e
ΔG_{gas}	−24.6539	−16.3099
ΔG_{solv}	11.3398	10.1038
ΔG_{total}	−13.3141	−6.2061

*3.1.3.4. 2-Oxo-N′-(4-phenylthiazol-2-yl)-2H-benzo[h] chromene-3-carbohydr-azide (**6d**).* This substance was obtained by heating coumarin **5d** (4 mmol, 1.25 g) and phenacyl bromide (4 mmol, 0.78 g) for 9 h and was purified from EtOH. Brown powder; yield: 36%; MP = 214–215 °C; IR (KBr) ν_{max}/cm^{-1} = 3247, 3191 (NH), 3058, 3025 (C–H sp^2), 1715 (coumarin C=O), 1642 (amidic C=O); ^{1}H-NMR (850 MHz, DMSO-d_6): δ_{ppm} = 7.29 (m, 2H, Ar-H_4 + thiazole-H_5), 7.39 (t, J = 7.65 Hz, 2H, Ar-$H_{3,5}$), 7.68 (t, J = 7.65 Hz, 3H, NH + Ar-$H_{2,6}$), 7.80 (t, J = 6.8 Hz, 1H, coumarin-H_8), 7.86 (t, J = 7.65 Hz, 1H, coumarin-H_9), 8.12 (d, J = 8.5 Hz, 2H, coumarin-H_{10}); 8.37 (d, J = 8.5 Hz, 1H, coumarin-H_7), 8.64 (d, J = 8.5 Hz, 1H, coumarin-H_8), 9.47 (s, 1H, coumarin-H_4), 9.96 (s, 1H, NH), 10.74 (s, 1H, amidic-NH); ^{13}C-NMR (212.5 MHz, DMSO-d_6): δ_{ppm} = 104.03 (thiazole-C_5), 113.07 (coumarin-C_3), 116.97 (coumarin-C_{4a}), 118.01 (coumarin-C_{10}), 122.89 (coumarin-C_5), 126.07 (coumarin-C_7), 127.15 (coumarin-C_6), 128.03 (coumarin-C_8), 129.07 (Ar-$C_{2,6}$), 129.34 (coumarin-C_{8a}), 129.48 (Ar-C_5), 129.58 (Ar-C_3), 129.65 (Ar-C_4), 130.48 (Ar-C_1), 135.04 (coumarin-C_{5a}), 136.57 (coumarin-C_9), 143.72 (coumarin C_4), 150.97 (thiazole-C_4), 155.11 (coumarin C_{10a}), 159.85 (coumarin-C=O), 162.15 (amidic C=O), 171.52 (thiazole-C_2); MS m/z (%): 413 (M^+, 18.62), 337 (17.21), 295 (16.70), 272 (19.69), 188 (100), 157 (13.03), 104 (41.57), 53 (30.16).

3.1.4. Synthesis of 2-cyano-N′-(4-phenylthiazol-2-yl) acetohydrazide (7). A mixture of compound **3** (6 mmol, 1 g) and 2-bromoacetophenone (6 mmol, 1.19 g) in ethanol (23 mL) and 0.1 mL of triethylamine was heated for 4 h. The adduct generated was gathered and purified by EtOH. Light yellow powder; yield: 55%; MP = 178–180 °C; IR (KBr) ν_{max}/cm^{-1} = 3270, 3195 (2NH), 3111, 3071 (C–H sp^2), 2955, 2862 (C–H sp^3), 2257 (CN), 1701 (C=O); ^{1}H-NMR (850 MHz, DMSO-d_6): δ_{ppm} = 3.82 (s, 2H, CH_2)**, 3.92 (s, 2H, CH_2)*, 7.28 (t, J = 7.4 Hz, 1H, Ar-H_4), 7.30 (s, 1H, thiazole-H_5), 7.38 (t, J = 7.65 Hz, 1H, Ar-$H_{3,5}$), 7.82 (d, J = 7.65 Hz, 1H, Ar-$H_{2,6}$), 9.66 (s, 1H, thiazole-NH)**,

9.74 (s, 1H, thiazole-NH)*, 10.15 (s, 1H, amidic-NH)*, 10.60 (s, 1H, amidic-NH)**; ^{13}C-NMR (212.5 MHz, DMSO-d_6): δ_{ppm} = 23.83 (CH_2)*, 24.36 (CH_2)**, 103.95 (thiazole-C_5)**, 104.94 (thiazole-C_5)*, 115.97 (CN)**, 116.24 (CN)*, 126.06 (Ar-$C_{3,5}$), 128.06 (Ar-C_4)**, 128.20 (Ar-C_4)*, 129.06 (Ar-$C_{2,6}$)**, 129.11 (Ar-$C_{2,6}$)*, 134.82 (Ar-C_1)*, 134.99 (Ar-C_1)**, 151.06 (thiazole-C_4)**, 151.43 (thiazole-C_4)*, 163.18 (amidic-C=O)**, 168.16 (amidic C=O)*, 171.58 (thiazole-C_2)*, 171.77 (thiazole-C_2)**; MS *m*/*z* (%): 258 (M^+, 14.05), 190 (13.52), 112 (23.25), 83 (41.90), 77 (100).

Signals are ascribed to * *syn* and ** to *anti* stereoisomers in this spectrum.

3.1.5 The alternative method to produce coumarin–thiazole hybrids 6a–d:. To a solution of thiazole **7** (38 mmol, 1 g) and salicylaldehyde derivatives (38 mmol) in EtOH (20 mL), 0.1 mL of piperidine was supplied. The solution was allowed to boil for 7–13 h and then poured onto cold water (20 mL) with 0.1 mL of HCl. The formed adducts were collected and purified by EtOH to furnish **6a–d**.

3.2. Antiproliferative evaluation

Three human tumor cells (MCF-7, HCT-116, and HepG2) and EA. hy926 as a normal human cell line was used for evaluation using sulforhodamine B (SRB) assay.[48–51] The cell lines were purchased from ATCC and cultured in RPMI-1640 with penicillin (100 U mL^{-1})–streptomycin (100 μg mL^{-1}) and heat-inactivated fetal bovine serum (10% v/v) at 37 °C and 5% (v/v) CO_2. The growing cells were trypsinized and cultured in a 96-well tissue culture plate for 24 h before being manipulated. Cells treated with compounds (0.01, 0.1, 1, 10, and 100 μg mL^{-1}) were mixed with the untreated (control) cells. Following 72 h of dosage exposure, the cells were fixed with 10% w/v TCA for an hour at 4 °C. Following many washes, cells were stained with a 0.4% (w/v) SRB solution for ten minutes in the dark. Glacial acetic acid, 1% (v/v), was used to eliminate any leftover discoloration residue. SRB-stained cells were dissolved in Tris–HCl and allowed to dry overnight before being submitted to a microplate reader to determine the color intensity at 540 nm.

3.3. Molecular docking simulations

The molecular docking simulation utilized the open-source PyRx (**https://pyrx.sourceforge.io/**) embedded Vina tool. The X-ray protein crystal of CDK2 was retrieved from the Protein Data Bank (RCSB: PDB) as PDB ID 3QTR.[46] The protein structure was prepared using the embedded DockPrep tool of Chimera17.1. This preparation tool includes the removal of unnecessary water, ions, and the co-crystallized ligand followed by adding hydrogen atoms and assigning charges to protein atoms. The tested derivatives were drawn and energy minimized using OSIRIS DataWarrior and then saved in sdf format (**https://openmolecules.org/datawarrior/**). The docking simulation utilized a grid box that contained the co-crystallized **X36** binding site using the default MMFF94x forcefield. The grid box dimensions were x = 17.4734 Å, y = 17.1954 Å and z = 15.9998 Å. The output binding conformations were visualized by BIOVIA Discovery Studio Visualizer 2021 (**https://discover.3ds.com/discovery-studio-visualizer-download**).

3.4. Molecular dynamics simulations

NAMD 3.0.0 was used for MD simulations applying Charmm-36 forcefield.[52,53] The protein chains were constructed using the QwikMD toolkit of the VMD software[53,54] and then checked for any missing hydrogens. The co-crystallized water molecules were eliminated and the protonation statuses of the amino acid residues were adjusted to *p*H = 7.4. After that, the entire structure was immersed in an orthorhombic TIP3P water box together with 0.15 M Na+ and Cl^- ions in a solvent buffer with a 20 Å thickness. The systems were then energy-minimized and equilibrated for five nanoseconds. The simulation was started for protein-ligand complexes using the top-scoring docked conformations of **5c** and **6c**. ForceField Toolkit (ffTK), was used to generate the compounds' topologies and properties. The binding free energy of the docked complex was calculated as reported using 100 frames according to the following equation.[55]

$$\Delta G_{binding} = \Delta G_{complex} - \Delta G_{receptor} - \Delta G_{inhibitor}$$

Each of the aforementioned terms requires the calculation of multiple energy components, including van der Waals energy, electrostatic energy, internal energy from molecular mechanics, and polar contribution to solvation energy.

4. Conclusion

In the present work, a series of novel thiazolyl–coumarin derivatives were synthesized, starting with 1-cyanoacetylthiosemicarbazide and characterized by spectral studies. The biological results of the synthesized derivatives revealed the privilege of the open-chain thioamides **5a–d** over their cyclized phenyl thiazole **6a–d** against the three cancerous cell lines. The molecular docking simulation explained the superiority of the coumarins **5c** and **6c** due to their ability to form extra H-bond with the hinge Asp145. The open chain **5c** showed an IC_{50} range of 4.5–7.5 μM while its thiazole congener **6c** demonstrated an IC_{50} range of 2.6–10.0 μM against the three tested cancerous cell lines. Nonetheless, **6c** exhibited a lower selectivity ratio than **5c** which showed normal EA.hy926 IC_{50} 8.4 μM compared to 26.6 μM of **5c.** In the same context, substituting the coumarin moiety with the cyano group in **7** managed to conserve the necessary binding pattern to the CDK2 hinge and hydrophobic pocket therefore, appreciated cytotoxicity was observed against the three cancerous cell lines (IC_{50} = 6.5–10.3 μM) with good selectivity ratio. Molecular dynamics simulations showed that **5c** exhibited superior stability with an average RMSD of 2.09 Å relative to 3.27 Å of **6c**. Moreover, the interaction energies of both **5c** and **6c** were evaluated, with mean values estimated at −65.38 kcal mol^{-1} and −52.44 kcal mol^{-1}, respectively. The investigation also highlighted the formation of stable hydrophilic contacts, especially hydrogen bonds, with both compounds forming between 1 and 3 hydrogen bonds during the simulation.

Conflicts of interest

The authors declare no conflict of interest.

Acknowledgements

The authors extend their appreciation to the Deanship of Research and Graduate Studies at King Khalid University for funding this work through small group research under grant number RGP1/53/45.

References

1 R. Gerosa, R. De Sanctis, F. Jacobs, C. Benvenuti, M. Gaudio, G. Saltalamacchia, R. Torrisi, G. Masci, C. Miggiano, F. Agustoni, P. Pedrazzoli, A. Santoro and A. Zambelli, *Crit. Rev. Oncol. Hematol.*, 2024, **196**, 104324.

2 K. L. Ferguson, S. M. Callaghan, M. J. O'Hare, D. S. Park and R. S. Slack, The Rb-CDK4/6 signaling pathway is critical in neural precursor cell cycle regulation, *J. Biol. Chem.*, 2000, **275**(43), 33593–33600.

3 L. Cen, B. L. Carlson, M. A. Schroeder, J. L. Ostrem, G. J. Kitange, A. C. Mladek, S. R. Fink, P. A. Decker, W. Wu, J.-S. Kim, T. Waldman, R. B. Jenkins and J. N. Sarkaria, p16-Cdk4-Rb axis controls sensitivity to a cyclin-dependent kinase inhibitor PD0332991 in glioblastoma xenograft cells, *Neuro-Oncology*, 2012, **14**(7), 870–881.

4 T. Chohan, H. Qian, Y. Pan and J.-Z. Chen, Cyclin-dependent kinase-2 as a target for cancer therapy: progress in the development of CDK2 inhibitors as anti-cancer agents, *Curr. Med. Chem.*, 2015, **22**, 237–263.

5 S. Tadesse, E. C. Caldon, W. Tilley and S. Wang, Cyclin-Dependent Kinase 2 Inhibitors in Cancer Therapy: An Update, *J. Med. Chem.*, 2019, **62**(9), 4233–4251.

6 C. Sánchez-Martínez, L. M. Gelbert, M. J. Lallena and A. De Dios, *Bioorg. Med. Chem. Lett.*, 2015, **25**, 3420–3435.

7 A. Huwe, R. Mazitschek and A. Giannis, Small molecules as inhibitors of cyclin-dependent kinases, *Angew. Chem., Int. Ed.*, 2003, **42**(19), 2122–2138.

8 K. Parang and G. Sun, Protein kinase inhibitors in drug discovery, *Drug Discovery Handbook*, ed. S. C. Gad, John Wiley & Sons Inc, 2005.

9 G. Lolli and L. N. Johnson, CAK-Cyclin-dependent activating kinase: a key kinase in cell cycle control and a target for drugs?, *Cell Cycle*, 2005, **4**, 572–577.

10 C. J. Sherr, G1 phase progression: cycling on cue, *Cell*, 1994, **79**(4), 551–555.

11 J. Pines and T. Hunter, Cyclin-dependent kinases: a new cell cycle motif?, *Trends Cell Biol.*, 1991, **1**(5), 117–121.

12 Y. Li, J. Zhang, W. Gao, L. Zhang, Y. Pan, S. Zhang and Y. Wang, Insights on structural characteristics and ligand binding mechanisms of CDK2, *Int. J. Mol. Sci.*, 2015, **16**, 9314–9340.

13 T. Nasr, S. Bondock and M. Youns, Anticancer activity of new coumarin substituted hydrazide-hydrazone derivatives, *Eur. J. Med. Chem.*, 2014, **76**, 539–548.

14 M. Riveiro, N. De Kimpe, A. Moglioni, R. Vazquez, F. Monczor, C. Shayo and C. Davio, Coumarins: old compounds with novel promising therapeutic perspectives, *Curr. Med. Chem.*, 2010, **17**, 1325–1338.

15 K. S. Kim, S. D. Kimball, R. N. Misra, D. B. Rawlins, J. T. Hunt, H.-Y. Xiao, S. Lu, L. Qian, W.-C. Han, W. Shan, T. Mitt, Z. -W. Cai, M. A. Poss, H. Zhu, J. S. Sack, J. S. Tokarski, C. Y. Chang, N. Pavletich, A. Kamath, W. G. Humphreys, P. Marathe, I. Bursuker, K. A. Kellar, U. Roongta, R. Batorsky, J. G. Mulheron, D. Bol, C. R. Fairchild, F. Y. Lee and K. R. Webster, Discovery of aminothiazole inhibitors of cyclin-dependent kinase 2: synthesis, X-ray crystallographic analysis, and biological activities, *J. Med. Chem.*, 2002, **45**, 3905–3927.

16 L.-Y. Li, J.-D. Peng, W. Zhou, H. Qiao, X. Deng, Z.-H. Li, J.-D. Li, Y.-D. Fu, S. Li, K. Sun, H.-M. Liu and W. Zhao, Potent hydrazone derivatives targeting esophageal cancer cells, *Eur. J. Med. Chem.*, 2018, **148**, 359–371.

17 A. Jashari, F. Imeri, L. Ballazhi, A. Shabani, B. Mikhova, G. Dräger, E. Popovski and A. Huwiler, Synthesis and cellular characterization of novel isoxazolo- and thiazolohydrazinylidene-chroman-2,4-diones on cancer and non-cancer cell growth and death, *Bioorg. Med. Chem.*, 2014, **22**, 2655–2661.

18 E. Schonbrunn and S. B. R. Alam, Development of highly potent and selective diaminothiazole inhibitors of cyclin-dependent kinases, *J. Med. Chem.*, 2013, **56**, 3768–3782.

19 S. S. A. El-Karim, Y. M. Syam, A. M. E. Kerdawy and T. M. Abdelghany, New thiazol-hydrazono-coumarin hybrids targeting human cervical cancer cells: Synthesis, CDK2 inhibition, QSAR and molecular docking studies, *Bioorg. Chem.*, 2019, **86**, 80–96.

20 A. M. El-Naggar, M. A. El-Hashash and E. B. Elkaeed, Eco-friendly sequential one-pot synthesis, molecular docking, and anticancer evaluation of arylidene–hydrazinyl–thiazole derivatives as CDK2 inhibitors, *Bioorg. Chem.*, 2021, **108**, 104615.

21 R. Balicki and P. Nantka-Namirski, Cancerostatics. Part V. Synthesis of some acyl hydrazine derivatives, *Acta Pol. Pharm.*, 1988, **45**(1), 1–7.

22 S. Bondock, N. Alabbad, A. Hossana and M. M. Abdou, 1-Cyanoacetylthiosemicarbazides: Recent advances in their synthesis, reactivity in heterocyclization, and bio-applications, *Mini-Rev. Org. Chem.*, 2024, **21**, 409–423.

23 H. Eyring, D. M. Grant and H. Hecht, The rotational barrier in ethane, *J. Chem. Educ.*, 1962, **39**(9), 466–468.

24 P. R. Rablen, Computational analysis of the solvent effect on the barrier to rotation about the conjugated C–N bond in methyl N, N-dimethylcarbamate, *J. Org. Chem.*, 2000, **65**(23), 7930–7937.

25 S. E. Barrows and T. H. Eberlein, Understanding rotation about a C=C double bond, *J. Chem. Educ.*, 2005, **82**(9), 1329–1333.

26 V. Kubyshkin and N. Budisa, Amide rotation trajectories probed by symmetry, *Org. Biomol. Chem.*, 2017, **15**(32), 6764–6772.

27 H. Friebolin, *Basic One-And Two-Dimensional NMR Spectroscopy*, John Wiley & Sons, 2010.

28 L. A. LaPlanche and M. T. Rogers, Cis and trans configurations of the peptide bond in N-monosubstituted

amides by nuclear magnetic resonance, *J. Am. Chem. Soc.*, 1964, **86**(3), 337–341.
29 G. W. Gribble and F. P. Bousquet, Deshielding effects in the NMR spectra of *ortho*-substituted anilides and thioanilides, *Tetrahedron*, 1971, **27**(16), 3785–3794.
30 S. Betzi, R. A. Alam and H. Han, *CDK2 in Complex with Inhibitor RC-1-148*, 2012, RCSB: Protein Data Bank: PDB.
31 E. Schonbrunn, S. Betzi, R. Alam, M. P. Martin, A. Becker, H. Han, R. Francis, R. Chakrasali, S. Jakkaraj, A. Kazi, S. M. Sebti, C. L. Cubitt, A. W. Gebhard, L. A. Hazlehurst, J. S. Tash and G. I. Georg, Development of highly potent and selective diaminothiazole inhibitors of cyclin-dependent kinases, *J. Med. Chem.*, 2013, **56**, 3768–3782.
32 E. W. Bell and Y. Zhang, DockRMSD: an open-source tool for atom mapping and RMSD calculation of symmetric molecules through graph isomorphism, *J. Cheminf.*, 2019, **11**, 40.
33 Y. Zhang, DockRMSD online, available from: **https://zhanggroup.org/DockRMSD/**.
34 Y. Li, J. Zhang, W. Gao, L. Zhang, Y. Pan, S. Zhang and Y. Wang, Insights on Structural Characteristics and Ligand Binding Mechanisms of CDK2, *Int. J. Mol. Sci.*, 2015, **16**, 9314–9340.
35 T. M. Sielecki, T. L. Johnson, J. Liu, J. K. Muckelbauer, R. H. Grafstrom, S. Cox, J. Boylan, C. R. Burton, H. Chen, A. Smallwood, C.-H. Chang, M. Boisclair, P. A. Benfield, G. L. Trainor and S. P. Seitz, Quinazolines as Cyclin Dependent Kinase Inhibitors, *Bioorg. Med. Chem. Lett.*, 2001, **11**, 1157–1160.
36 A. A. Russo, P. D. Jeffrey and N. P. Pavletich, Structural basis of cyclin-dependent kinase activation by phosphorylation, *Nat. Struct. Biol.*, 1996, **3**, 696–700.
37 A. Daina, O. Michielin and V. Zoete, SwissADME: a free web tool to evaluate pharmacokinetics, drug-likeness and medicinal chemistry friendliness of small molecules, *Sci. Rep.*, 2017, **7**, 42717.
38 Available from: **https://www.swissadme.ch/index.php**.
39 C. Lipinski, Lead- and Drug Like Compounds: The Rule of Five Revolution, *Drug Discovery Today: Technol.*, 2004, **1**, 337–341.
40 Y. C. Martin, A bioavailability score, *J. Med. Chem.*, 2005, **48**(9), 3164–3170.
41 D. F. Veber, S. R. Johnson, H.-Y. Cheng, B. R. Smith, K. W. Ward and K. D. Kopple, Molecular Properties That Influence the Oral Bioavailability of Drug Candidates, *J. Med. Chem.*, 2002, **45**(12), 2615–2623.
42 A. Daina and V. Zoete, A BOILED-Egg to predict gastrointestinal absorption and brain penetration of small molecules, *ChemMedChem*, 2016, **11**, 1117–1121.
43 W. J. Egan, K. M. Merz and J. Baldwin, Prediction of Drug Absorption Using Multivariate Statistics, *J. Med. Chem.*, 2000, **43**, 3867–3877.
44 A. Daina, O. Michielin and V. Zoete, iLOGP: a simple, robust, and efficient description of *n*-octanol/water partition coefficient for drug design using the GB/SA approach, *J. Chem. Inf. Model.*, 2014, **54**(12), 3284–3301.
45 C. A. Lipinski, F. Lombardo, B. W. Dominy and P. J. Feeney, Experimental and computational approaches to estimate solubility and permeability in drug discovery and development settings, *Adv. Drug Deliv. Rev.*, 2001, **23**, 3–25.
46 J. H. Lin and M. Yamazaki, Role of P-Glycoprotein in Pharmacokinetics: Clinical Implications, *Clin. Pharmacokinet.*, 2003, **42**, 59–98.
47 F. J. Sharom, ABC multidrug transporters: structure, function and role in chemoresistance, *Pharmacogenomics*, 2008, **9**, 105–127.
48 S. Bondock, T. Albarqi, M. M. Abdou and N. M. Mohamed, Computational insights into novel benzenesulfonamide-1,3,4-thiadiazole hybrids as a possible VEGFR-2 inhibitor: design, synthesis and anticancer evaluation with molecular dynamics studies, *New J. Chem.*, 2023, **47**, 20602–20618.
49 S. Bondock, T. Albarqi, T. Nasr, N. M. Mohamed and M. M. Abdou, Design, synthesis, cytotoxic evaluation and molecular docking of novel 1,3,4-thiadiazole sulfonamides with azene and coumarin moieties as carbonic anhydrase inhibitors, *Arabian J. Chem.*, 2023, **16**, 104956.
50 S. Bondock, T. Albarqi, I. A. Shaaban and M. M. Abdou, Novel asymmetrical azines appending 1,3,4-thiadiazole sulfonamide: synthesis, molecular structure analyses, *in silico* ADME, and cytotoxic effect, *RSC Adv.*, 2023, **13**, 10353–10366.
51 S. Bondock, T. Albarqi, M. Abboud, T. Nasr, N. M. Mohamed and M. M. Abdou, Tail-approach based design, synthesis, and cytotoxic evaluation of novel disubstituted and trisubstituted 1,3-thiazole benzenesulfonamide derivatives with suggested carbonic anhydrase IX inhibition mechanism, *RSC Adv.*, 2023, **13**, 24003–24022.
52 J. C. Phillips, R. Braun, W. Wang, J. C. Gumbart, E. Tajkhorshid, E. Villa, C. Chipot, R. D. Skeel, L. V. Kalé and K. Schulten, Scalable molecular dynamics with NAMD, *J. Comput. Chem.*, 2005, **26**, 1781–1802.
53 J. V. Ribeiro, R. C. Bernardi, T. Rudack, K. Schulten and E. Tajkhorshid, QwikMD-Gateway for Easy Simulation with VMD and NAMD, *Biophys. J.*, 2018, **114**(3), 673a–674a.
54 W. Humphrey, A. Dalke and K. Schulten, VMD: visual molecular dynamics, *J. Mol. Graphics*, 1996, **14**(1), 33–38.
55 B. R. Miller, T. D. McGee, J. M. Swails, N. Homeyer, H. Gohlke and A. E. Roitberg, MMPBSA. py: an efficient program for end-state free energy calculations, *J. Chem. Theory Comput.*, 2012, **8**, 3314–3321.